The Arpege project at Météo-France.

Philippe Courtier Catherine Freydier Jean-François Geleyn
Florence Rabier Michel Rochas

Météo-France
Paris, France.

Summary: The Arpege project intends to provide Météo-France with an operational NWP system for the 90's. The code development is achieved in cooperation with ECMWF (IFS project). The main features are a global spectral model with variable resolution, both an optimal interpolation and a 3-D variational analysis and a consistent water cycle.

In addition to the NWP applications, the code is designed as a research tool. In particular the tangent-linear and adjoint versions of the model have been developed allowing for the investigation of 4-D variational assimilation. A Kalman filter is also implemented and provision is made for studying the most unstable modes of the flow.

The model is the basis of the French Climate Community Model with in particular ozone (or other passive variables) as historical variable.

1 Introduction.

Météo-France relies for its medium range forecasts on the products disseminated by ECMWF and concentrates its NWP efforts on the short-range (0–72 h) but at the meso-α scale (35 km). For comparison, the shortest half wavelength resolved by the current ECMWF model is 190 km (95 at truncation 213). The current operational system consists of a limited area model (PERIDOT) whose lateral boundary conditions are given by a large scale global model: EMERAUDE. A description of the strengths and weaknesses of PERIDOT has been presented by Geleyn at the 1987 ECMWF seminar and is described in Imbard et al. (1987). His main conclusions were :

- *The system should be judged as a result of pioneering effort and thus only as a promising first step in a new area of numerical weather prediction;*
- *Objective verification indicates a better skill for surface parameters than that of the EMERAUDE forecast;*
- *The improvement (modest for moisture, larger for temperature, and substantial for wind) coincides with an independent measure of usefulness (relative to natural variability) for the same surface parameters;*

• *Most of this specific meso-scale skill is the result of adaptation to orography and land surface forcing but more marginal improvements are apparently resulting from the special meso-scale features of the data assimilation procedure and from "physical forcing";*

• *Sometimes unexpected meso-scale predictability (either by its scale or its range) becomes apparent; this might indicate that spectacular progress could be achieved in coming years (like the 70's - 80's explosion of synoptic scale predictability) but the examples are too rare to be conclusive on this account.*

Finally we can identify four main areas of problems that are likely to slow down the above-mentionned forthcoming progress:

a) The negative influence of lateral boundary conditions;

b) The erratic character of deep convective forcing and its too great scale dependency in the models;

c) The fact that increased resolution beyond mesh sizes of about 50 km does not seem to bring anything more than better adaptation to local orography (one should keep in mind that this may only be a consequence of (b), but this point needs further investigation);

d) The necessity of having the most coherent (and thus most expensive) data assimilation system to blend large-scale and meso-scale observed informations.

From these positive results of the PERIDOT system and from the identification of its main weaknesses, Météo-France decided to launch a NWP project for the 90's: the Arpege project. In order to avoid the lateral boundary conditions problem in the forecast and more important, in the data-assimilation, it has been decided that the system were to be global. The feasability study of a global variable resolution spectral model has been conducted by Courtier and Geleyn (1988) along the ideas of Schmidt (1977). The semi-Lagrangian scheme was then a necessity to avoid a too short time step incompatible with the operational constraints.

In order to prepare the future evolution of NWP, it has then be decided that Arpege should have to be a test-bed both for the introduction of liquid water and for variational assimilation. The short term consequences were, firstly the necessity of a consistent water cycle both from the mass, momentum and energy point of view and secondly the necessity of the development of the adjoint of the model.

Described like this, the project was likely to be too ambitious for a single NWP center. Since the 1988 4-year plan of ECMWF required the same type of NWP tools, a cooperation for a common development of a code was set-up by the Heads of Research of both institutes (Dave Burridge for ECMWF and Frédéric Delsol for Météo-France). The algorithmic part of these projects is the subject of the present paper, with results showing the feasibility of the chosen options.

The operational commitment of Météo-France for the 90's is the meso-α scale. However, results obtained by Ducrocq and Bougeault (1990) indicate that we should not consider point (c) of Imbard

et al. (1987) too pessimistic. In other words, as the potential of the meso-β scale (10 km) has been demonstrated in case studies, Météo-France has decided that the second half of the 90's will see an operational assessment on a routine basis of this potential, attempting at reproducing 10 years later the success of the PERIDOT bet but at the 10 km scale.

2 The model.

2.1 Model equations.

In the following, cycle 7 of the model is described. The main modifications with respect to cycle 6 are the u-v formulation and the Legendre transforms.

2.1.1 Eulerian formulation of the primitive equations.

We use as vertical coordinate the pressure based hybrid coordinate η following the orography decribed by Simmons and Burridge (1981). The following relationships hold

$$\left.\begin{aligned} \eta(0,\pi) &= 0 \\ \eta(\pi,\pi) &= 1 \\ \frac{\partial \eta}{\partial p}(p,\pi) &> 0 \end{aligned}\right\} \tag{1}$$

Where π is the surface pressure. The hydrostatic equation reads

$$\frac{\partial \Phi}{\partial \eta} = -\frac{RT}{p}\frac{\partial p}{\partial \eta} \tag{2}$$

which is used as a diagnostic equation in order to compute the geopotential Φ at level p through an integration in the vertical from the lower boudary condition $\Phi(\pi) = \Phi_s$, where Φ_s denotes the surface geopotential (g times the orography).

The evolution of the parameters which define the atmospheric state in the model, horizontal wind $\vec{v}$, temperature T and specific humidity q_v is governed by the following equations.

Momentum equation

$$\frac{d\vec{v}}{dt} + 2\vec{\Omega} \times \vec{v} + RT\nabla \ln p + \nabla\Phi = -g\frac{\partial \eta}{\partial p}\frac{\partial \vec{F}_{\vec{v}}}{\partial \eta} + \vec{K}_{\vec{v}} \tag{3}$$

Thermodynamic equation

$$\frac{dT}{dt} - \kappa T\frac{\omega}{p} = -\frac{g}{c_p}\frac{\partial \eta}{\partial p}\frac{\partial F_h}{\partial \eta} + K_h \tag{4}$$

Moisture equation

$$\frac{dq_v}{dt} = -g\frac{\partial \eta}{\partial p}\frac{\partial F_{q_v}}{\partial \eta} + K_{q_v} \tag{5}$$

The right hand side terms of the equations (3), (4) and (5) are the vertical fluxes F provided by the subgrid scale parameterizations and the horizontal diffusion K of momentum, enthalpy and specific humidity. We assume that both dry air and water vapor are perfect gases and we shall now consider the consequences of this assumption. Following Gill (1982), since dry air is composed mostly (99 %) of diatomic molecules and water vapor of triatomic molecules one has

$$c_{pa} = \frac{7}{2}R_a \qquad c_{pv} = 4\,R_v$$

where R_a and R_v are respectively the gas constants for dry air and water vapor, and c_{pa} and c_{pv} the specific heats at constant pressure of dry air and water vapor. The atmosphere being a mixture of dry air and water vapor, R and c_p are given by

$$R = R_a q_a + R_v q_v$$

$$c_p = c_{pa} q_a + c_{pv} q_v$$

where q_a is the specific dry air content. Since we assume (von Bezold, 1888) that the liquid and solid phases of water which appear in the atmosphere are immediately removed by precipitation, one has $q_a = 1 - q_v$. In order to have a fully consistent thermodynamical cycle, the saturated partial pressure of water vapor over water, e_s and ice e_g are computed from the integration of the Clausius-Clapeyron relation

$$\frac{1}{e_s}\frac{de_s}{dT} = \frac{L_v}{R_v T^2} \qquad \frac{1}{e_g}\frac{de_g}{dT} = \frac{L_s}{R_v T^2}$$

where L_v and L_s are the latent heats of vaporization and sublimation respectively. We have assumed that the specific volumes of the condensed phases of water are negligible and thus set equal to zero. These formulas are accurate in the meteorological range of temperature when the two latent heats are linear functions of temperature

$$L_v(T) = L_v(T_t) + (c_{pv} - c_l)(T - T_t) \qquad L_s(T) = L_s(T_t) + (c_{pv} - c_g)(T - T_t)$$

where T_t is the temperature of the triple point of water, c_l and c_g are the specific heats at constant pressure of liquid water and ice. Thus

$$e_s(T) = e_s(T_t)\exp\left\{\left[L_v(0)\left(\frac{1}{T_t} - \frac{1}{T}\right) + (c_l - c_{pv})\ln\frac{T_t}{T}\right]/R_v\right\} \tag{6}$$

$e_g(T)$ is obtained from (6) changing L_v and c_l into L_s and c_g.

Classically, as there is no source term in the continuity equation, a fictitious substitution process is supposed to occur in order to conserve the total mass of the atmosphere. The mass of water which is removed from the atmosphere by precipitation is replaced by an equivalent amount of dry air, the reverse process taking place when water vapor is supplied to the atmosphere by evaporation at the surface of the Earth. As an option we can avoid to perform this approximation; the continuity equation then reads

$$\frac{\partial}{\partial \eta}\left(\frac{\partial p}{\partial t}\right) + \nabla \cdot \left(\vec{v}\frac{\partial p}{\partial \eta}\right) + \frac{\partial}{\partial \eta}\left(\dot{\eta}\frac{\partial p}{\partial \eta}\right) = -g\frac{\partial F_p}{\partial \eta} \tag{7}$$

F_p denotes the mass flux due to precipitation/evaporation. Through vertical integration, one obtains the evolution equation for surface pressure using, $gF_p(1) + gE$ as lower boundary condition for the mass flux ($F_p(1)$ denotes the precipitation which fall on the ground and E the evaporation flux at the surface)

$$\frac{\partial \pi}{\partial t} = -\int_0^1 \nabla \cdot \left(\vec{v}\frac{\partial p}{\partial \eta}\right) d\eta - gF_p(1) - gE \tag{8}$$

the pressure coordinate vertical velocity

$$\omega = -\int_0^\eta \nabla \cdot \left(\vec{v}\frac{\partial p}{\partial \eta}\right) d\eta + \vec{v}\cdot\nabla p - gF_p(\eta) \tag{9}$$

and the vertical velocity

$$\dot{\eta}\frac{\partial p}{\partial \eta} = -\frac{\partial p}{\partial t} - \int_0^\eta \nabla \cdot \left(\vec{v}\frac{\partial p}{\partial \eta}\right) d\eta - gF_p(\eta) \tag{10}$$

Expressed in terms of the physical components u and v of the wind field, the equations over the sphere Σ of radius a become

$$\left.\begin{aligned}
&\frac{\partial u}{\partial t} - v\zeta + v\nabla^u v + u\nabla^u u + \dot{\eta}\frac{\partial u}{\partial \eta} - fv + RT\nabla^u \ln p + \nabla^u \Phi = -g\frac{\partial \eta}{\partial p}\frac{\partial F_{\vec{v}}^u}{\partial \eta} + K_{\vec{v}}^u \\
&\frac{\partial v}{\partial t} + vD + u\nabla^u v - v\nabla^u u + \frac{u^2+v^2}{a}\tan\theta + \dot{\eta}\frac{\partial v}{\partial \eta} + fu + RT\nabla^v \ln p + \nabla^v \Phi \\
&\qquad\qquad = -g\frac{\partial \eta}{\partial p}\frac{\partial F_{\vec{v}}^v}{\partial \eta} + K_{\vec{v}}^v \\
&\frac{\partial T}{\partial t} + u\nabla^u T + v\nabla^v T + \dot{\eta}\frac{\partial T}{\partial \eta} - \kappa T\frac{\omega}{p} = -\frac{g}{c_p}\frac{\partial \eta}{\partial p}\frac{\partial F_h}{\partial \eta} + K_h \\
&\frac{\partial q_v}{\partial t} + u\nabla^u q_v + v\nabla^v q_v + \dot{\eta}\frac{\partial q_v}{\partial \eta} = -g\frac{\partial \eta}{\partial p}\frac{\partial F_{q_v}}{\partial \eta} + K_{q_v}
\end{aligned}\right\} \tag{11}$$

θ denotes the latitude and $\nabla^u A$ (respectively $\nabla^v A$) denotes the physical component of the gradient of a given field A in the direction u (respectively v). Their expressions are given by

$$\nabla^u A = \frac{1}{a\cos\theta}\frac{\partial A}{\partial \lambda} \tag{12}$$

$$\nabla^v A = \frac{1}{a}\frac{\partial A}{\partial \theta} \tag{13}$$

2.1.2 Relations between wind, vorticity and divergence.

The wind is computed from the velocity potential χ and the stream function ψ

$$\vec{v} = \nabla\chi + \nabla \times \psi \tag{14}$$

which are easily derived from vorticity and divergence through the Poisson equations

$$\chi = \Delta^{-1} D \tag{15}$$

$$\psi = \Delta^{-1} \zeta \tag{16}$$

In these last three relationships (14), (15) and (16), the kernel of the Laplacian operator is implicitely assumed to reduce to the constant functions. It is then equivalent to know vorticity and divergence or the wind vector. This property is obviously satisfied over the sphere. The divergence of a vector field $\vec{B}$ of physical components B^u and B^v is given by

$$\nabla \cdot \vec{B} = \frac{1}{a\cos\theta}\left\{\frac{\partial B^u}{\partial \lambda} + \frac{\partial B^v \cos\theta}{\partial \theta}\right\} \tag{17}$$

and the rotational

$$\nabla \times \vec{B} = \frac{1}{a\cos\theta}\left\{\frac{\partial B^v}{\partial \lambda} - \frac{\partial B^u \cos\theta}{\partial \theta}\right\} \tag{18}$$

Remark: The expressions of the physical components u and v of the wind field $\vec{v}$ are the following

$$u = \frac{1}{a\cos\theta}\left(\frac{\partial \chi}{\partial \lambda} - \cos\theta \frac{\partial \psi}{\partial \theta}\right) \tag{19}$$

$$v = \frac{1}{a\cos\theta}\left(\frac{\partial \psi}{\partial \lambda} + \cos\theta \frac{\partial \chi}{\partial \theta}\right) \tag{20}$$

2.2 Horizontal discretization.

2.2.1 Representation of the fields.

The horizontal variations of the prognostic variables and of the orography are represented by truncated series of surface spherical harmonics

$$X(\lambda, \mu, \eta, t) = \sum_{n=0}^{N} \sum_{m=-n}^{n} X_n^m(\eta, t)\, Y_n^m(\lambda, \mu) \tag{21}$$

where λ denotes longitude, μ the sine of latitude θ and Y_n^m the surface spherical harmonic of degree n and order m

$$Y_n^m(\lambda, \mu) = P_n^m(\mu)\, e^{im\lambda}$$

the P_n^m are the associated Legendre functions of the first kind, defined by

$$P_n^m(\mu) = \sqrt{(2n+1)\frac{(n-m)!}{(n+m)!}}\frac{1}{2^n n!}\left(1-\mu^2\right)^{m/2}\frac{d^{n+m}}{d\mu^{n+m}}\left(\mu^2-1\right)^n \qquad m \geq 0$$

and

$$P_n^{-m}(\mu) = P_n^m(\mu)$$

With these definitions, one has

$$\frac{1}{4\pi}\iint_\Sigma Y_n^m \bar{Y}_r^s \, d\lambda \, d\mu = \delta_{(n=r)}\delta_{(m=s)}$$

$\bar{Y}$ is the complex conjugate of Y and $\delta_{(n=r)}$ the Kronecker delta function which is equal to 1 if $n = r$ and 0 otherwise. The X_n^m are the complex value spectral coefficients of the field X given by

$$X_n^m(\eta,t) = \frac{1}{4\pi}\iint_\Sigma X(\lambda,\mu,\eta,t)\bar{Y}_n^m(\lambda,\mu)\, d\lambda \, d\mu \tag{22}$$

Since X is real, X_n^{-m} is the complex conjugate of X_n^m. In (21), we have used a triangular truncation since triangular truncations are invariant through a rotation of the pole of coordinate. Use of this property is done in the variable resolution version of the model, see Rochas et al. (1991b) for the transformation of the coefficients in a such a rotation.

In order to compute the tendencies of the model, the transform method introduced by Orszag (1970), and applied to the primitive equations by Eliasen et al. (1970) is used. The right-hand-sides of the equations are evaluated on a Gaussian grid which consists of $K \geq \frac{3}{2}N+1$ latitudes circles and $J \geq 3N+1$ longitudes. This grid allows no aliasing in the quadratic terms. Furthemore Hortal and Simmons (1991) have shown that it is possible to use a reduced Gaussian grid, the number of points on a latitude circle being reduced such that the distance between two adjacent points remains approximatively constant and equal to its value at the equator $2\pi a/J$. Such a reduced grid is implemented in the code.

2.2.2 Inverse transforms.

Fields.

All the variables and their horizontal derivatives are evaluated on the collocation grid through spectral transforms, inverse Legendre followed by inverse Fourier

$$X_m(\mu_k) = \sum_{n=|m|}^{N} X_n^m P_n^m(\mu_k) \tag{23}$$

$$X(\lambda_j,\mu_k) = \sum_{m=-N}^{N} X_m(\mu_k)\, e^{im\lambda_j} \tag{24}$$

the last sum is performed using Fast Fourier Transform.

Derivation with respect to longitude.

The derivation with respect to λ is performed in Fourier space (multiplication by im).

Derivation with respect to latitude.

For the derivatives of a field A with respect to θ a special procedure is applied following Temperton (1991), we first compute the spectral components of

$$\left\{a\cos\theta\frac{1}{a}\frac{\partial A}{\partial\theta}\right\}_n^m = -(n-1)\varepsilon_n^m A_{n-1}^m + (n+2)\varepsilon_{n+1}^m A_{n+1}^m \tag{25}$$

with

$$\varepsilon_n^m = \sqrt{\frac{n^2-m^2}{4n^2-1}} \tag{26}$$

then, the grid point values are obtained using inverse Legendre and inverse Fourier transforms. Wind components are computed in a similar manner using

$$\{a\cos\theta u\}_n^m = im\chi_n^m + (n-1)\varepsilon_n^m\psi_{n-1}^m - (n+2)\varepsilon_{n+1}^m\psi_{n+1}^m \tag{27}$$

$$\{a\cos\theta v\}_n^m = im\psi_n^m - (n-1)\varepsilon_n^m\chi_{n-1}^m + (n+2)\varepsilon_{n+1}^m\chi_{n+1}^m \tag{28}$$

Remark 1: In the Legendre transform, the summation over n for a given m is from 0 to $N+1$ whereas m still varies from 0 to N.

Remark 2: In the semi-Lagrangian formulation (section 2.5), the vorticity is no longer needed on the grid. The availability of vorticity on the grid is controlled by a logical LVOR, if the model is Eulerian, LVOR is reset to .TRUE., vorticity is also needed if one is interested in advection diagnostics or in potential vorticity post-processing.

Remark 3: The divisions by $a\cos\theta$ are performed in Fourier space.

Computation of pole values.

The analysis (OI and 3-D var) and the semi-Lagrangian advection scheme require for the horizontal interpolation an extension of the grid point arrays north of row 1 and south of row K.

Row 0 of the grid point arrays can either be located at the pole or be a clever duplication of row 1. This is controlled by a logical LPOLE. When LPOLE is set to false, row 0 contains the value of row 1 at relative longitude π. Accordingly, row -1 contains the value of row 2 (1 if LPOLE is true) at relative longitude π. For the vectors, the sign of both the u and v component has to be changed since the local frame of reference is extended along a meridian by continuity. The theoretical advantage of having a point at the pole is to preserve the continuity at order 1 instead of 0 across the pole in the horizontal interpolations.

When LPOLE is true, the pole values are computed using the following formulas valid for $\mu = \pm 1$ and $m \geq 0$

$$A^m(\mu = \pm 1) = \delta_{(m=0)} \sum_{n=0}^{N} A_n^0 P_n^0(\mu) \tag{29}$$

$$(\nabla^u A)^m(\mu = \pm 1) = \delta_{(m=1)} \frac{i}{2a} \mu \sum_{n=1}^{N} A_n^1 \sqrt{n(n+1)}\, P_n^0(\mu) \tag{30}$$

$$(\nabla^v A)^m(\mu = \pm 1) = -\delta_{(m=1)} \frac{1}{2a} \sum_{n=1}^{N} A_n^1 \sqrt{n(n+1)}\, P_n^0(\mu) \tag{31}$$

and for the wind components

$$u^m = \delta_{(m=1)} \frac{1}{2a} \sum_{n=1}^{N} \left(i\mu\chi_n^1 + \psi_n^1\right) \sqrt{n(n+1)}\, P_n^0(\mu) \tag{32}$$

$$v^m = \delta_{(m=1)} \frac{1}{2a} \sum_{n=1}^{N} \left(-\chi_n^1 + i\mu\psi_n^1\right) \sqrt{n(n+1)}\, P_n^0(\mu) \tag{33}$$

In addition the equations (11) remain valid at the poles with the metric term set to 0 and the Fourier components of the "horizontal derivatives" of the wind given by

$$(\nabla^u u)^0 = \frac{1}{2} D \tag{34}$$

$$(\nabla^u v)^0 = \frac{1}{2} \zeta \tag{35}$$

$$(\nabla^u u)^2 = -\frac{1}{4}(A - iB) \tag{36}$$

$$(\nabla^u v)^2 = -\frac{i\mu}{4}(A - iB) \tag{37}$$

where A and B are the two components of the deformation

$$A - iB = \frac{1}{a^2} \sum_{n=2}^{N} \left(\chi_n^2 - i\mu\psi_n^2\right) \sqrt{(n-1)n(n+1)(n+2)}\, P_n^0(\mu) \tag{38}$$

and

$$P_n^0(\mu = \pm 1) = \mu^n \sqrt{2n+1} \tag{39}$$

Remark: μP_n^0 has the same symmetry property with respect to the equator as P_n^1. P_n^0 has the reverse symmetry property with respect to the equator as P_n^1.

2.2.3 Direct transforms.

The result of the grid point computations is transformed back into the spectral space, using first Fast Fourier Transforms to compute the Fourier coefficients on the Gaussian latitudes

$$Z_m(\mu_k) = \frac{1}{J} \sum_{1}^{J} Z(\lambda_j, \mu_k)\, e^{-im\lambda_j} \tag{40}$$

and then the Gaussian quadrature formula to compute the spectral coefficients (provision has also been made for a Lobatto quadrature)

$$Z_n^m = \sum_{k=1}^{K} \varpi_k Z_m(\mu_k) P_n^m(\mu_k) \tag{41}$$

where the the Gaussian abscissas, μ_k, are the roots of the Legendre polynomial of degree K

$$P_K(\mu_k) = 0$$

and the Gaussian weights ϖ_k given by

$$\varpi_k = \frac{1-\mu_k^2}{[K P_{K-1}(\mu_k)]^2}$$

Vorticity and divergence are obtained from wind using, in spectral space

$$\zeta_n^m = im\left\{\frac{v}{a\cos\theta}\right\}_n^m - n\,\varepsilon_{n+1}^m\left\{\frac{u}{a\cos\theta}\right\}_{n+1}^m + (n+1)\,\varepsilon_n^m\left\{\frac{u}{a\cos\theta}\right\}_{n-1}^m \tag{42}$$

$$D_n^m = im\left\{\frac{u}{a\cos\theta}\right\}_n^m + n\,\varepsilon_{n+1}^m\left\{\frac{v}{a\cos\theta}\right\}_{n+1}^m - (n+1)\,\varepsilon_n^m\left\{\frac{v}{a\cos\theta}\right\}_{n-1}^m \tag{43}$$

Remark. In (42) and (43) have been introduced the two quantities

$$\left\{\frac{u}{a\cos\theta}\right\}_n^m = \sum_{k=1}^{K} \varpi_k \left\{\frac{u}{a\cos\theta}\right\}^m (\mu_k) P_n^m(\mu_k) \tag{44}$$

$$\left\{\frac{v}{a\cos\theta}\right\}_n^m = \sum_{k=1}^{K} \varpi_k \left\{\frac{v}{a\cos\theta}\right\}^m (\mu_k) P_n^m(\mu_k) \tag{45}$$

It must be clear that since $\frac{u}{a\cos\theta}$ and $\frac{v}{a\cos\theta}$ have infinite expansions, $\left\{\frac{u}{a\cos\theta}\right\}_n^m$ and $\left\{\frac{v}{a\cos\theta}\right\}_n^m$ do not represent the coefficients of the development of $\frac{u}{a\cos\theta}$ and $\frac{v}{a\cos\theta}$ in spherical harmonics, it should only be considered as a crude approximation. However, with the relations (44) and (45), the equations (42) and (43) are algebraically equivalent to the traditional form

$$\zeta_n^m = \sum_{k=1}^{K} \frac{\varpi_k}{a(1-\mu_k^2)} \left\{ im\,(v\cos\theta)^m P_n^m(\mu_k) + (u\cos\theta)^m \left(1-\mu_k^2\right) \frac{dP_n^m}{d\mu}(\mu_k) \right\} \tag{46}$$

$$D_n^m = \sum_{k=1}^{K} \frac{\varpi_k}{a(1-\mu_k^2)} \left\{ im\,(u\cos\theta)^m P_n^m(\mu_k) - (v\cos\theta)^m \left(1-\mu_k^2\right) \frac{dP_n^m}{d\mu}(\mu_k) \right\} \tag{47}$$

As pointed out by Temperton (1991) equations (46) and (47) require formally four Legendre transforms whereas only two are necessary with equations (44) and (45).

2.2.4 Variable resolution.

A conformal transform of the η-surfaces is introduced. The horizontal fields are spectrally expanded in the basis functions defined on the transformed sphere. The equations are kept the same as set (11). The output (input) of the inverse (direct) transforms are the pseudo-wind $\vec{v}'$ and the derivatives ∇' defined by

$$\vec{v} = m\vec{v}'$$
$$\nabla = m\nabla'$$

where ∇' is the same formal operator as ∇, but on the transformed sphere. The Poisson equations become

$$\chi = \Delta'^{-1}\frac{D}{m^2} \tag{48}$$

$$\psi = \Delta'^{-1}\frac{\zeta}{m^2} \tag{49}$$

where Δ'^{-1} is the same formal operator as Δ^{-1} but over the transformed sphere. As a consequence, the state variables of the model are $\zeta' = \zeta/m^2$ and $D' = D/m^2$ for momentum variables (or equivalently ψ and χ).

In order to keep the grid point computations (CPG) almost identical, the vorticity and the divergence are computed from the pseudo-divergence and the pseudo-vorticity at the beginning of CPG and same for the wind and the derivatives. The only modifications which remain are in the semi-implicit adjustment where the divergence (respectively the derivatives) will have to be multiplied by $(\bar{m}/m)^2$ (respectively $\bar{m}/m$) (see Courtier and Geleyn (1988) for the choice of $\bar{m}$, value of the mapping factor, taken constant over the sphere, used in the linear operator behind the semi-implicit). These modifications are detailed in subsection 2.4.

2.3 Vertical discretization.

The vertical coordinate η varies from 0 at the top of the atmosphere, where $p = 0$, to 1 at the surface, where $p = \pi$. The atmosphere is divided into L layers unevenly spaced relative to pressure. The layers are defined by the pressure at their interfaces

$$p_{\tilde{l}} = A_{\tilde{l}} + B_{\tilde{l}}\pi \tag{50}$$

The model does not require pressure to be defined at model's levels, however this is necessary for the specification of initial conditions and post-processing where it is defined as the mean pressure over

the layer. In the following we denote by δ the variation of a quantity across a layer, for instance

$$\delta p_\ell = p_{\tilde{\ell}} - p_{\tilde{\ell}-1}$$

2.3.1 Hydrostatic equation.

In order to integrate the hydrostatic equation, temperature is assumed to be constant within a layer

$$\Phi_{\tilde{\ell}} = \Phi_s + \sum_{k=L}^{\ell+1} R_k T_k \ln\left(\frac{p_{\tilde{k}}}{p_{\tilde{k}-1}}\right) \tag{51}$$

$$\Phi_\ell = \Phi_{\tilde{\ell}} + \alpha_\ell R_\ell T_\ell \tag{52}$$

where

$$\alpha_\ell = 1 - \frac{p_{\tilde{\ell}-1}}{\delta p_\ell} \ln\left(\frac{p_{\tilde{\ell}}}{p_{\tilde{\ell}-1}}\right) \tag{53}$$

and $\alpha_1 = 1$. Equation (52) is obtained from (51) by discretizing

$$\Phi_\ell = \frac{\delta_\ell (p\,\Phi)}{\delta p_\ell} + R_\ell T_\ell$$

2.3.2 Vertical velocity.

The continuity equation is discretized as

$$\frac{\partial}{\partial t}\delta p_\ell = -\delta p_\ell D_\ell - \delta B_\ell \vec{v}_\ell \cdot \nabla\pi - \delta w_\ell$$

where $w = \dot{\eta}\frac{\partial p}{\partial \eta}$. Summing over a vertical leads to the surface pressure evolution equation

$$\frac{\partial \pi}{\partial t} = -\sum_{\ell=1}^{L} (\delta p_\ell D_\ell + \delta B_\ell \vec{v}_\ell \cdot \nabla\pi)$$

In addition, integrating the continuity equation provides w

$$w_{\tilde{\ell}} = -\sum_{k=1}^{\ell} (\delta p_k D_k + \delta B_k \vec{v}_k \cdot \nabla\pi) - B_{\tilde{\ell}} \frac{\partial \pi}{\partial t} \tag{54}$$

2.3.3 Vertical advections.

In the Eulerian versions the vertical advections of velocity, temperature and specific humidity are computed using

$$\left(w\frac{\partial X}{\partial p}\right)_\ell = \frac{1}{2\delta p_\ell}\left(w_{\tilde{\ell}}(X_{\ell+1} - X_\ell) + w_{\tilde{\ell}-1}(X_\ell - X_{\ell-1})\right)$$

which is the result of the discretization of

$$w\frac{\partial X}{\partial p} = \frac{\partial wX}{\partial p} - X\frac{\partial w}{\partial p}$$

using $X_{\tilde{\ell}} = \frac{1}{2}(X_\ell + X_{\ell+1})$.

2.3.4 Pressure gradient force.

In order to derive an angular momentum conserving scheme, the pressure gradient force is discretized into

$$\begin{aligned} \nabla\Phi + RT\nabla \ln p &= \nabla\Phi_s \\ &+ \sum_{k=L}^{\ell+1} \left[\ln\left(\frac{p_{\tilde{k}}}{p_{\tilde{k}-1}}\right) \nabla\left(R_k T_k\right) \right] + \alpha_\ell \nabla\left(R_\ell T_\ell\right) \\ &+ \left\{ \sum_{k=L}^{\ell+1} \left[R_k T_k \left(\frac{B_{\tilde{k}}}{p_{\tilde{k}}} - \frac{B_{\tilde{k}-1}}{p_{\tilde{k}-1}} \right) \right] + R_\ell T_\ell \frac{B_{\tilde{\ell}}}{p_{\tilde{\ell}}} \right\} \nabla\pi \end{aligned} \tag{55}$$

with

$$\nabla\left(R_\ell T_\ell\right) = \left(R_v - R_a\right) T_\ell \nabla q_{v\ell} + R_\ell \nabla T_\ell \tag{56}$$

2.3.5 Energy conversion term.

The discretization of energy conversion term is obtained through

$$\frac{RT}{p}\omega = -\omega\frac{\partial\Phi}{\partial p} = -\frac{\partial\omega\Phi}{\partial p} + \Phi\frac{\partial\omega}{\partial p}$$

where ω is computed using

$$\omega = \frac{\partial p}{\partial t} + \vec{v}\cdot\nabla p + \dot{\eta}\frac{\partial p}{\partial \eta} = \vec{v}\cdot\nabla p - \int_0^\eta \nabla\cdot\left(\vec{v}\frac{\partial p}{\partial\eta}\right) d\eta$$

which gives

$$\left(\frac{\omega}{p}\right)_\ell = \vec{v}_\ell \left(\frac{1}{p}\nabla p\right)_\ell - \frac{1}{\delta p_\ell}\left[\alpha_\ell \left(\delta p_\ell D_\ell + \delta B_\ell \vec{v}_\ell\cdot\nabla\pi\right) + \ln\left(\frac{p_{\tilde{\ell}}}{p_{\tilde{\ell}-1}}\right) \sum_{k=1}^{\ell-1} \left(\delta p_k D_k + \delta B_k \vec{v}_k\cdot\nabla\pi\right) \right]$$

The energetical consistency of the vertical discretization has been shown by Simmons and Burridge (1981).

2.4 Time discretization.

The time scheme is a leapfrog semi-implicit scheme which is formulated as a correction to the explicit leapfrog scheme

$$\left.\begin{aligned} \pi^{\tau+1} &= \mathcal{P} - \beta\Delta t\,\nu\left(D'^{\tau+1} - 2D'^{\tau} + D'^{\tau-1}\right)\bar{m}^2 \\ \zeta'^{\tau+1} &= \nabla'\times\mathcal{U}' \\ D'^{\tau+1} &= \nabla'\cdot\mathcal{U}' - \beta\Delta t\,\Delta'\left[\gamma\left(T^{\tau+1} - 2T^{\tau} + T^{\tau-1}\right) + \mu\left(\pi^{\tau+1} - 2\pi^{\tau} + \pi^{\tau-1}\right)\right] \\ T^{\tau+1} &= \mathcal{T} - \beta\Delta t\tau\left(D'^{\tau+1} - 2D'^{\tau} + D'^{\tau-1}\right)\bar{m}^2 \\ q_v^{\tau+1} &= \mathcal{Q} \end{aligned}\right\} \tag{57}$$

$\mathcal{P}$, $\mathcal{U}' = \mathcal{U}/m$, $\mathcal{T}$ and $\mathcal{Q}$ are the values which would be calculated respectively for surface pressure, wind, temperature and specific humidity using the explicit scheme (which can be obtained putting $\beta = 0$ in the above system). The four operators γ, τ, ν and μ are obtained through the linearization of finite difference operators relative to an isothermal reference state of rest defined by $\bar{T}$ and $\bar{\pi}$

$$(\gamma T)_\ell = \bar{\alpha}_\ell R_a T_\ell + \sum_{k=\ell+1}^{L} R_a T_k \ln \frac{\bar{p}_{\bar{\ell}}}{\bar{p}_{\bar{\ell}-1}} \tag{58}$$

$$(\tau D)_\ell = \frac{R_a \bar{T}}{c_{pa}} \left[\bar{\alpha}_\ell D_\ell + \frac{1}{\delta \bar{p}_\ell} \left(\ln \frac{\bar{p}_{\bar{\ell}}}{\bar{p}_{\bar{\ell}-1}} \right) \sum_{k=1}^{\ell-1} \delta \bar{p}_k D_k \right] \tag{59}$$

$$\nu D = \sum_{\ell=1}^{L} \delta \bar{p}_\ell D_\ell \tag{60}$$

$$\mu \pi = \frac{R_a \bar{T}}{\bar{\pi}} \pi \tag{61}$$

where $\bar{p}$ is computed using (50) with the value $\bar{\pi}$ of the surface pressure and $\bar{\alpha}$ using (53) with the value $\bar{p}$ of pressure. It should be pointed out that these operators commute with the ∇' operator. The set of equations (57) is transformed in

$$\left.\begin{aligned} \pi^{\tau+1} + \beta \Delta t \bar{m}^2 \nu D'^{\tau+1} &= \mathcal{P}^* \\ \zeta'^{\tau+1} &= \nabla' \times \mathcal{U}^{*\prime} \\ D'^{\tau+1} + \beta \Delta t \, \Delta' \left(\gamma T^{\tau+1} + \mu \pi^{\tau+1} \right) &= \nabla' \cdot \mathcal{U}^{*\prime} \\ T^{\tau+1} + \beta \Delta t \bar{m}^2 \tau D'^{\tau+1} &= \mathcal{T}^* \\ q_v^{\tau+1} &= \mathcal{Q} \end{aligned}\right\} \tag{62}$$

with in (62)

$$\left.\begin{aligned} \mathcal{P}^* &= \mathcal{P} - \beta \Delta t \nu \left(-2D^\tau + D^{\tau-1} \right) \frac{\bar{m}^2}{m^2} \\ \mathcal{U}^* &= \mathcal{U} - \beta \Delta t \nabla \left[\gamma \left(-2T^\tau + T^{\tau-1} \right) + \mu \left(-2\pi^\tau + \pi^{\tau-1} \right) \right] \\ \mathcal{T}^* &= \mathcal{T} - \beta \Delta t \tau \left(-2D^\tau + D^{\tau-1} \right) \frac{\bar{m}^2}{m^2} \end{aligned}\right\} \tag{63}$$

$\mathcal{P}^*$, $\mathcal{U}^* = m\mathcal{U}^{*\prime}$ and $\mathcal{T}^*$ are computed in grid-point space and then transformed to spectral space. Elimination of temperature and surface pressure in (62) leads to an equation for divergence

$$\left\{ 1 - \beta^2 \Delta t^2 \bar{m}^2 \, \mathrm{B} \Delta' \right\} D'^{\tau+1} = \nabla' \cdot \mathcal{U}^{*\prime} - \beta \Delta t \, \Delta' (\gamma \mathcal{T}^* + \mu \mathcal{P}^*) \tag{64}$$

where the operator B

$$\mathrm{B} = \gamma \tau + \mu \nu$$

is also used to compute the vertical normal modes used in non linear normal mode initialization. Temperature and surface pressure are deduced from divergence using (62). The set of equation described above uses π as historical variable represented in spectral space. As an option $\ln \pi$ can also be the historical variable, apart from obvious modifications in CPG, the operators μ and ν are modified in

$$\nu D = \frac{1}{\bar{\pi}} \sum_{\ell=1}^{L} \delta \bar{p}_\ell D_\ell \tag{65}$$

$$\mu \pi = R_a \bar{T} \ln \pi \tag{66}$$

A weak time filter is used after Asselin (1972), but which can be uncentered. If $\bar{X}$ denotes the filtered value of X

$$\bar{X}^\tau = X^\tau + \epsilon_1 \left(\bar{X}^{\tau-1} - X^\tau \right) + \epsilon_2 \left(X^{\tau+1} - X^\tau \right) \tag{67}$$

A Matsuno time scheme which is used in Kalman filter applications has also been implemented in the adiabatic version of the model.

2.5 Semi-Lagrangian.

A semi-implicit semi-Lagrangian scheme has been implemented following the original ideas of Robert (1982), comparizon with other formulations can be found in Rochas et al. (1991c) in the shallow-water context. As already said a point is introduced on the collocation grid at the pole in order to preserve the continuity of the fields at order 1 in the interpolations. For details on the formulation and/or the implementation, we refer to Hortal (1991), same volume.

2.6 Normal mode initialisation.

A mixed implicit/explicit nonlinear normal mode initialisation scheme has been implemented, along the ideas of Temperton (1989). It allows to compute the modes in a limited truncation (e.g. 42), saving both disk storage and computer time. The results are almost identical to the pure explicit scheme.

In the variable resolution case, the separability between the N-S and the E-W directions is lost. The following procedure, described by Marquet (1991), is applied

(1) The tendencies are first rotated in spectral space in order to have the pole of stretching at the same place as the pole of the colocation grid (see Rochas et al., 1991b, for stable spectral space rotation formulae).

(2) They are unstretched, again in spectral space. They are then represented in a truncation $N \times C$ which would be 450 for a T126C3.5 model (see Rochas et al., 1991a).

(3) Another rotation in spectral space is applied in order to have the pole at the northern pole.

(4) The nonlinear normal mode increments can then be computed using a mixed explicit/implicit scheme. It should be noted that a pure explicit scheme would lead to a too cumbersome scheme.

(5) The reverse rotations and unstretching are applied in order to obtain the NNMI increments back in spectral space over the transformed sphere.

One should note that each step is separable either at total wavenumber n as for the rotations or at zonal wavenumber m as for the unstretching or the computations of the NNMI increments.

The diabatic scheme is implemented in homogeneous and variable resolution configurations.

2.7 Physics.

2.7.1 Generalities.

The Arpege package is entirely derived, for its basic algorithms, from the physics used in the current large-scale spectral model at Météo-France, EMERAUDE described by Coiffier et al. (1987). However, the code has been fully rewritten for the following reasons :

- To obtain at the same time "plug-compatibility" of the physics calculation, following the rules of Kalnay et al. (1989), and a clean interface with the model's dynamics — in particular for the memory handling, for the consistent computation of geopotential, gas constants and specific- and latent heats as well as for the use of the physics' output —.
- To allow several possible uses of the physics' output within the dynamical model without any modification of the parameterization routines. As a consequence the transportable part of the physical routines produces only fluxes (all counted positive downwards, the orientation of the vertical axis being imposed by the vertical coordinate) and the computation of time tendencies is among the roles of the calling routines. Accordingly, diagnostics are of the extensive and not intensive type (mass weighted budget equations).
- To ensure transparency of the physics we impose the three following rules : (i) no numerical value is set-up in any physics computational routine; (ii) these routines use only implicit information on the actual distribution of the vertical levels; (iii) the only vertical coordinates known by the parameterization routines are pressure and geopotential.

In order to have readily access to the option to have a source term in the continuity equation due to precipitation/evaporation (equations (7) to (10)), several specific measures had to be taken in the Arpege implementation. Firstly, physics has to be called before dynamics. Secondly, to fulfil linear stability conditions in the case of semi-Lagrangian advection, the physics is entirely computed at $t - \Delta t$, all routines working in parallel from that point of view (there is of course still a need of

information transfer between them). When some input is needed from dynamical tendencies (so-called dynamical part of the moisture convergence in the convective closure assumption as only example up to now) a preliminary Eulerian computation is done before the call to physics' routines.

2.7.2 Moist thermodynamics' specificities.

The inherent non-linearity of the saturation specific humidity function $q_s(T,p)$ makes it necessary, even when neglecting the time variations of pressure, to use iterative Newton-type algorithms in order to find (T, q_v) solutions to the coupled set of equations expressing exact saturation of the final state as well as conservation of enthalpy, either at constant geopotential (stratiform condensation-evaporation process) or along the vertical (moist adiabatic ascent to be used in the deep convection calculations).

It is interesting to note as Geleyn et al. (1991) that taking into account both the variation of c_p with q_v and that of L_v with T in the course of such processes allows to build simpler algorithms for the Newton-type loops than when only one of the two effects is considered.

Indeed, starting from initial values T_0, q_{v0}, c_{p0} and L_{v0} one readily gets in the stratiform case

$$c_p = c_{p0} + (c_{pv} - c_l)(q_v - q_{v0})$$

and

$$L_v = L_{v0} + (c_{pv} - c_l)(T - T_0)$$

which coupled with

$$c_p dT + L_v dq_v = 0$$

leads to

$$L_v c_p = L_{v0} c_{p0}$$

the result being also valid in presence of ice instead of liquid water. Linearizing the saturation function for each iteration and eliminating the quadratic terms for the temperature iterative increments leads to the following symmetric algorithm

$$\left.\begin{aligned} q_{vi+1} - q_{vi} &= \frac{q_s(T_i,p) - q_{vi}}{1 + \frac{L_{vi}}{c_{pi}} \frac{dq_s(T_i,p)}{dT}} \\ c_{pi+1} - c_{pi} &= (c_{pv} - c_l)(q_{vi+1} - q_{vi}) \\ T_{i+1} - T_i &= -\frac{L_{vi}}{c_{pi+1}}(q_{vi+1} - q_{vi}) \\ L_{vi+1} - L_{vi} &= (c_{pv} - c_l)(T_{i+1} - T_i) \end{aligned}\right\} \quad (68)$$

For the moist adiabatic case the situation is a bit more complicated since one has to consider both a transport from the base of an atmospheric model slab (subscript "b") to the top (subscript "t") and the associated change of geopotential (at fixed pressures by definition). Nevertheless, choosing to do the whole Newton-type loop at "t", and considering the property

$$L_v c_p + (c_{pv} - c_l)(\Phi_t - \Phi_b) = L_{vb} c_{pb}$$

we obtain a very similar algorithm

$$\left.\begin{aligned} q_{vi+1} - q_{vi} &= \frac{q_s(T_i, p_t) - q_{vi}}{1 + \frac{\tilde{L}_i}{\tilde{c}_{pi}} \frac{dq_s(T_i, p_t)}{dT}} \\ \tilde{c}_{pi+1} - \tilde{c}_{pi} &= \left(c_{pv} - c_l + \tilde{R}_{vt}\right)(q_{vi+1} - q_{vi}) \\ T_{i+1} - T_i &= -\frac{\tilde{L}_i}{\tilde{c}_{pi+1}}(q_{vi+1} - q_{vi}) \\ \tilde{L}_{i+1} - \tilde{L}_i &= \left(c_{pv} - c_l + \tilde{R}_{vt}\right)(T_{i+1} - T_i) \end{aligned}\right\} \tag{69}$$

with

$$\left.\begin{aligned} \tilde{c}_p &= c_p + \tilde{R}_{bt} + \tilde{R}_{vt}(q_v - q_{vb}) \\ \tilde{L} &= L_v + \tilde{R}_{vt} T \end{aligned}\right\} \tag{70}$$

and where the change of geopotential $\Phi_t - \Phi_b$ depends on T_b, q_{vb}, T_t and q_{vt} only through three iteration-independent parameters of the type $R\, d\ln p$, ($\tilde{R}_{bb}$, $\tilde{R}_{bt}$ and $\tilde{R}_{vt}$), chosen from the model vertical coordinate discretization so that

$$\Phi_t - \Phi_b = \tilde{R}_{bb} T_b + \left[\tilde{R}_{bt} + \tilde{R}_{vt}(q_{vt} - q_{vb})\right] T_t \tag{71}$$

Concerning the $q_s(T,p)$ and $\frac{dq_s(T,p)}{dT}$ functions, we had to cater for an additional difficulty, namely to avoid that q_s may become absurd if $e_s(T) \geq p$, a fact that would happen if the formula for $e_s(T) < p$ is applied in a straightforward fashion. Choosing arbitrarily q_s to be equal to $e_s(T)/p$ in the case $e_s(T) \geq p$ allows to obtain an economical solution to this problem

$$q_s(T,p) = \frac{\Gamma}{1 + (R_v/R_a - 1)\max(0, 1 - \Gamma)}$$

$$\frac{dq_s}{dT}(T,p) = \frac{q_s(1 - q_s)}{1 - \Gamma} \frac{d\ln e_s(T)}{dT}$$

with

$$\Gamma = \frac{e_s(T)}{p}$$

2.7.3 Special algorithmic properties of the Arpege parameterization set.

It would be outside the scope of this paper to describe all the methods used in the design of the physics' package. References to the literature will replace that, while we shall concentrate on a few original items of the algorithms. The order of presentation of the phenomena will correspond to the order in which the routines are called: radiation first because its output is needed for vertical exchange calculations (including shallow convection) which just follow; gravity wave drag third as the next big influence on momentum and which uses some stability computation of the previous item; deep convection which takes some input from moisture turbulent vertical fluxes; stratiform condensation/evaporation as the other precipitation flux generator (and sharing with deep convection some of the above-mentioned preliminary thermodynamic computations); and finally soil hydrology following the last two items for the obvious reason that precipitations are needed beforehand, the temperature part of the continental soil evolution having been included in the vertical exchange part under the assumption of constant soil water content for the current time-step. Additionally a diagnostic computation of temperature moisture and wind at meteorological heights within the lowest model layer is performed following Geleyn (1988).

Radiation. The scheme used is complete but at the same time very cheap, by current standards. It is both an extension and a simplification of the methods described in Geleyn and Hollingsworth (1979) with optical properties synthesized in a few coefficients, following methods similar to those of Ritter and Geleyn (1991); an outline of the main practical characteristics of the implementation (in EMERAUDE) can be found in Cariolle et al. (1990).

From the algorithmic point of view the only interesting part is the solution of the so-called adding-method (to transform local transmissivities, reflectivities and emissivities for each layer into a flux computation on the whole vertical slab) ; the idea is here to write the full linear system in a matrix form and to solve the resulting linear system with a Gaussian elimination/back-substitution method but taking carefully into account the very sparse character of the matrix. This allows a 50% saving against more classical methods for that part.

Vertical exchange calculations. The exchange and drag coefficients for heat and for momentum are computed according to Louis et al. (1982) while the shallow convection is parameterized with a slightly modified version of Geleyn (1987). In fact the shallow convection is now only possible in conditionaly unstable situations.

The equations are treated with a full split implicit scheme for the atmosphere while the interaction with the surface over continental areas is taken into account in a rather original fashion. The equation for land surface temperature T_s, taken from a Deardorff (1978) force-restore-type method, is fully

linearized for all terms involving not only T_s itself but also the temperature and the specific humidity at the model's lowest level. Thus the linear system of the split implicit method is of order 2L+1 and is solved from top level temperature to top level humidity with a quite complex set of equations for the three middle variables T_L, T_s, q_{vL}, the matrix remaining however tridiagonal. This method similar to the "j" scheme mentioned in Kalnay and Kanamitsu (1988) has several advantages against a further split of the set of equations at the time of the linearization. As already mentioned, one assumes for obvious practical reasons equality between precipitation (yet to be computed) and evaporation (part of the implicit solution) at that stage.

Gravity wave drag. The scheme used is a modified version of the scheme of Boer et al. (1984), where the Lindzen's saturation criterium is explicitly used to compute momentum deposition (assuming exact saturation at the level of surface generation).

From the algorithmic point of view two points are worth mentioning. Firstly, we use consistent stability parameters between calculations of the vertical exchange coefficient and of the Brunt-Väisälä frequency in case of active shallow convection. Secondly, a correction is applied to the final fluxes in order to prevent either an acceleration or a change of sign of the projection of any wind vector on the surface "generating" wind. This restriction (Royer, personal communication) avoids a rare instability detected once in a climatic run and probably activated through vertical staggering problems between fluxes and variables used to compute them. A further algorithmic implementation point will be treated in section 2.8.1.

Deep convection. The scheme used is described in Bougeault (1985) with a few algorithmic enhancements.

Unlike for thermodynamic variables, there is no self regulating mechanism for the momentum mixing term $K(\vec{v}_c - \vec{v})$ in

$$\frac{d\vec{v}}{dt} = -M_c \frac{d\vec{v}}{dp} + K(\vec{v}_c - \vec{v})$$

where $\vec{v}_c$ are constant values obtained from momentum integral conservation properties once M_c and K are known from the thermodynamical part of the scheme. K is in addition constant along the vertical (and computed from the moist static energy budget). For linear stability, one has to use a split implicit scheme, which means that K is replaced in this simplified case of a single coefficient by

$$K' = K/(1 + K\delta t)$$

in the case of momentum equations, δt being the physics time-step.

To avoid a spurious positive feed-back between vertical diffusion and deep convection, the contribution of the dry static energy turbulent vertical mixing must be vertically averaged before being substracted from the convective tendency.

The solution for the mass-flux advective part of the equations for u, v, $s = c_pT + \Phi$ and q_v is treated with the semi-implicit stable diagonal-dominant and integral preserving algorithm of Geleyn et al. (1982). However, unlike in their case, there is nothing ensuring that in the entraining part of the cloud ascent $-\frac{dM_c}{dp}$ remains smaller than the physics time-step. This may induce non-linear instability, which indeed happened sporadically at the beginning of the operational implementation in EMERAUDE. The idea to cure the problem is to modify the previously computed mass-flux $M_{c\tilde{\ell}}$ at level $\tilde{\ell}$ according to

$$M'_{c\tilde{\ell}} - M'_{c\tilde{\ell}-1} = \frac{\left(M_{c\tilde{\ell}} - M'_{c\tilde{\ell}-1}\right)\left(\delta p_\ell + \delta t M'_{c\tilde{\ell}-1}\right)}{\delta p_\ell + \delta t \mid M_{c\tilde{\ell}} - M'_{c\tilde{\ell}-1} \mid}$$

a formulation which simulates quite closely what would have been achieved with a fully implicit scheme.

Stratiform condensation/evaporation. The simplified Kessler type scheme which we are using relies on the following hypothesis: all condensed water is precipitated within one time step ; evaporation can take place in unsaturated underlying layers according to

$$\frac{\partial\sqrt{F_p}}{\partial p} = \frac{K_{ev}}{p^2}(q_v - q_w)$$

where F_p is the precipitation rate, q_w the wet bulb specific humidity and K_{ev} a tunable parameter.

The algorithm has been written to take efficiently into account the symmetric roles of q_w in condensation and evaporation (limit not to be passed, i.e. just the condensate falls out and no oversaturation of sub cloud layers occurs).

Soil hydrology. Here a force-restore method is also used with no special feature.

2.8 Results.

2.8.1 Semi-Lagrangian integrations.

Different experiments have been performed in order to validate the semi-Lagrangian formulation. Figure 1 presents the 500 hPa geopotential map produced by a five day forecast of Arpege in T79L15 configuration with a time step length of 960 s. Figure 2 presents the same but for a semi-Lagrangian run with a 2400 s time step. The gravity wave drag is switched off since an instability occurred in the semi-Lagrangian runs (even at truncation T21) which has been traced back to an instability in the gravity wave drag parameterization. Since then the problem has been solved following Simmons (personal communication) and Hortal (1991) treating implicitly the terms proportional to the surface wind. The RMS of the differences is 260 J/kg, five time smaller than the typical RMS of error of a 5 day forecast. Similar positive results have been obtained in a winter case.

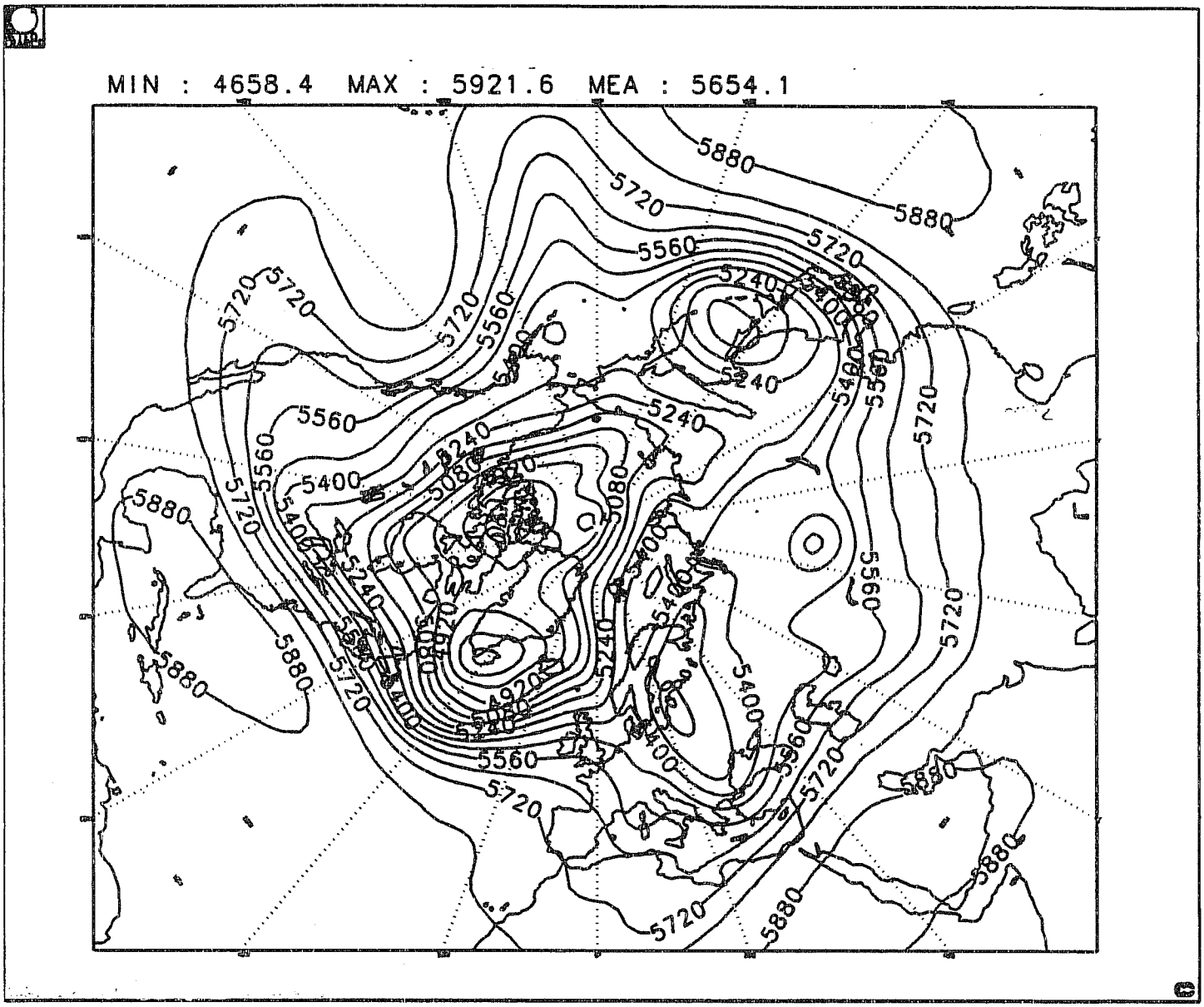

Fig. 1 *5 day forecast produced by the Eulerian (ζ, D) formulation of Arpege T79L15, time step length: 960 s, initial conditions : EMERAUDE initialized analysis. 500 hPa post processed geopotential.*

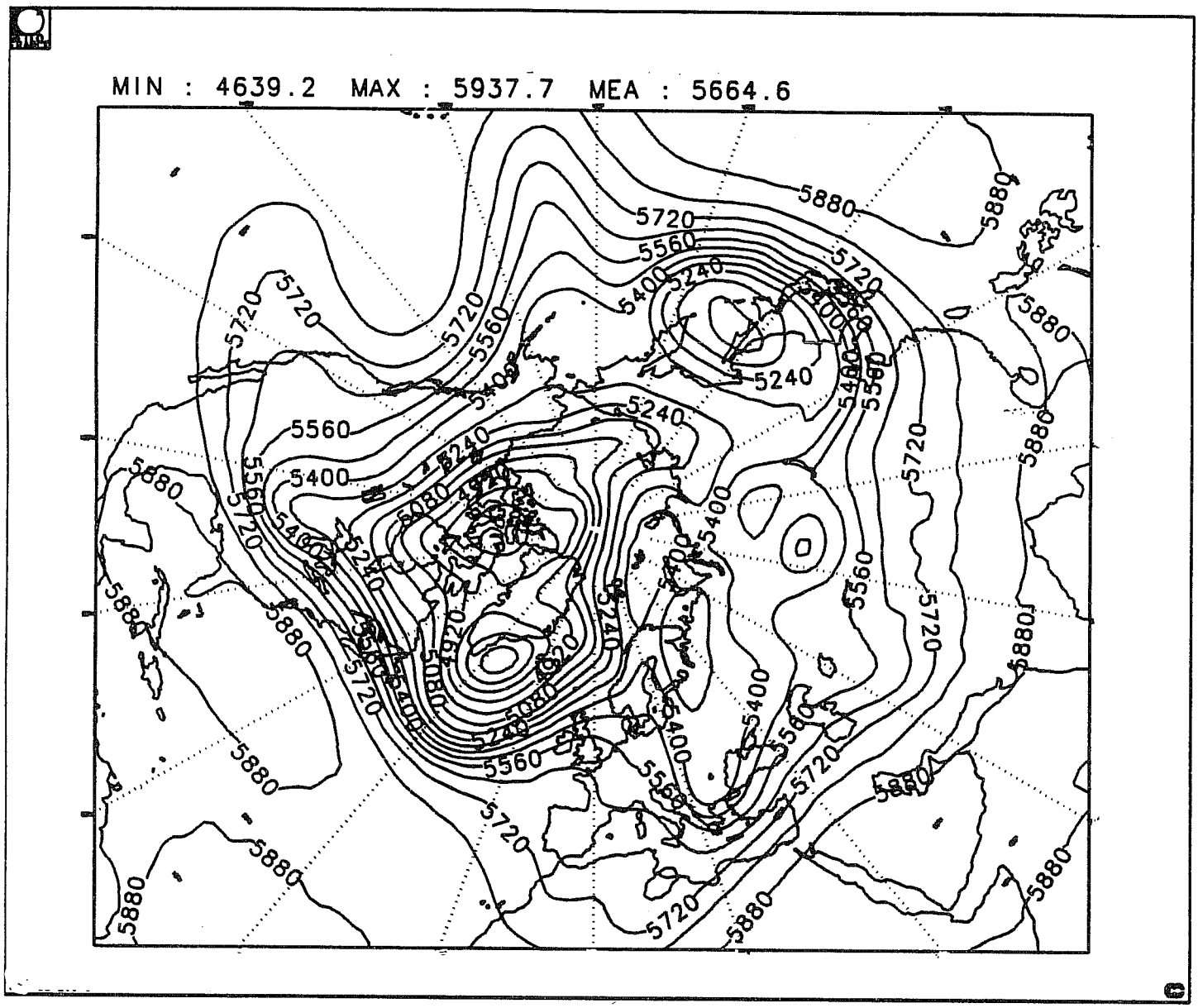

Fig. 2 *5 day forecast produced by the semi-Lagrangian formulation of Arpege T79L15, time step length: 2400 s, initial conditions : EMERAUDE initialized analysis. 500 hPa post processed geopotential.*

In early July, we conducted a short (too short since the move to Toulouse of the operational services took place this summer) parallel run of Arpege T79L15 in semi-Lagrangian configuration with the operational EMERAUDE system. The results obtained this winter from the parallel run involving Arpege T79L15 in Eulerian configuration are confirmed: the new model has a quality comparable to the EMERAUDE model when the same horizontal and vertical resolution is used. The impact in terms of scores is neutral with a day to day variability which has not been traced back to any particular problem in neither the old or the new system.

2.8.2 Variable resolution integrations.

The life cycle of a baroclinic wave on the sphere is chosen for the validation of the variable resolution since as pointed out by Simmons and Hoskins (1978) (from now SH78) it represents one of the main features of mid-latitude atmospheric dynamics. The basic zonal flow chosen symmetric about the equator is presented in Figure 3. A baroclinic zone centered at 45° latitude is characterized by a horizontal temperature gradient with a ground level temperature variation of 20 K from 30° to 60°, in geostrophic balance with a tropospheric jet whose maximum reaches 36 ms^{-1} at 150 hPa. This jet is baroclinically unstable and, for each zonal wavenumber the most unstable mode can be determined as the mode emerging after a long-range integration of a numerical model in the linear regime. As in SH78, zonal wavenumber six or height was chosen because, first, it is among the fastest growing modes and, second, because its wavelength (3600 to 4700 km at mid-latitudes) is close to the observed large-scale cyclone horizontal size.

The nonlinear evolution of the baroclinic wave is simulated by integrating the model for six days from initial conditions consisting of the zonal flow perturbed by the most unstable mode at zonal wavenumber height. Three configuration of the model are used: T42L19C1, T106L19C1 and T42L19C3, the results are presented respectively on Figure 4, 5 and 6. C1 means that the resolution is homogeneous over the sphere whereas C3 means that the resolution is equivalent to a T126 at the pole of stretching and T14 at the antipodes. The wave pattern obtained is typical of baroclinic instability and the large scale of the perturbation is similar both in the T42 and the T106 runs. However fine scale structures are visible at truncation 106 like the strong gradient in the cold front and the presence of a well marked warm front. The variable resolution T42C3 result is identical to the T106 result in the area of maximum resolution whereas in the area of low resolution it is close to the T42 forecast. This result is a spectacular confirmation, in the baroclinic instability case, of the earlier results obtained by Courtier and Geleyn (1988) using the shallow-water equations. If one remembers that we were considering a six day range, the interest of a variable resolution model which was clear for short range

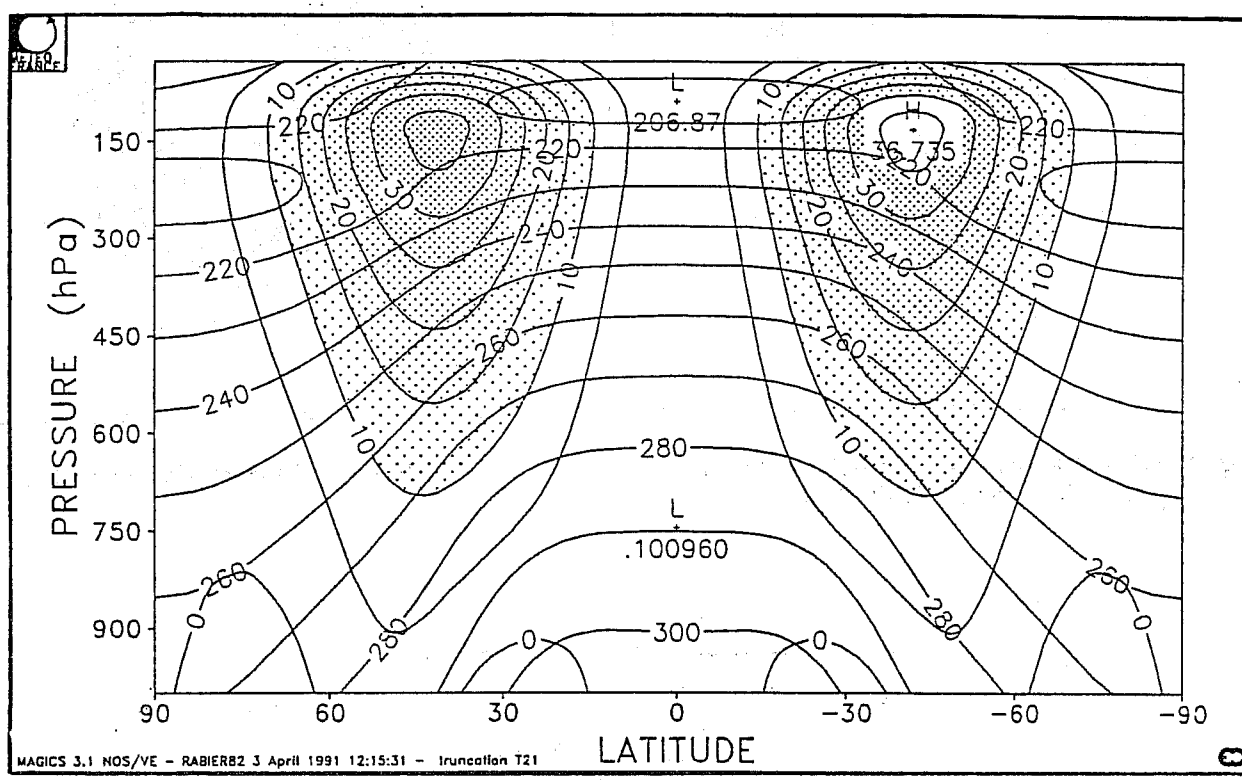

Fig. 3 *Latitude-height section showing temperature and zonal velocity for the basic state. Temperature contours are drawn every 10 K and zonal velocity contours are drawn every 5 ms^{-1}. Areas where winds exceed 10 ms^{-1} are shaded.*

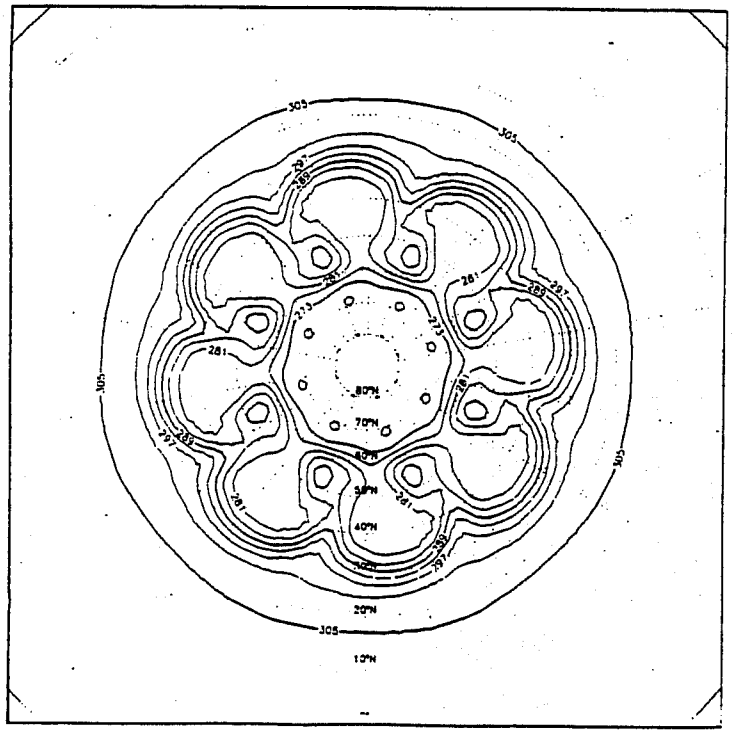

Fig. 4 : *1000 hPa temperature, result of a six day forecast T42L19C1, contour interval 4K.*

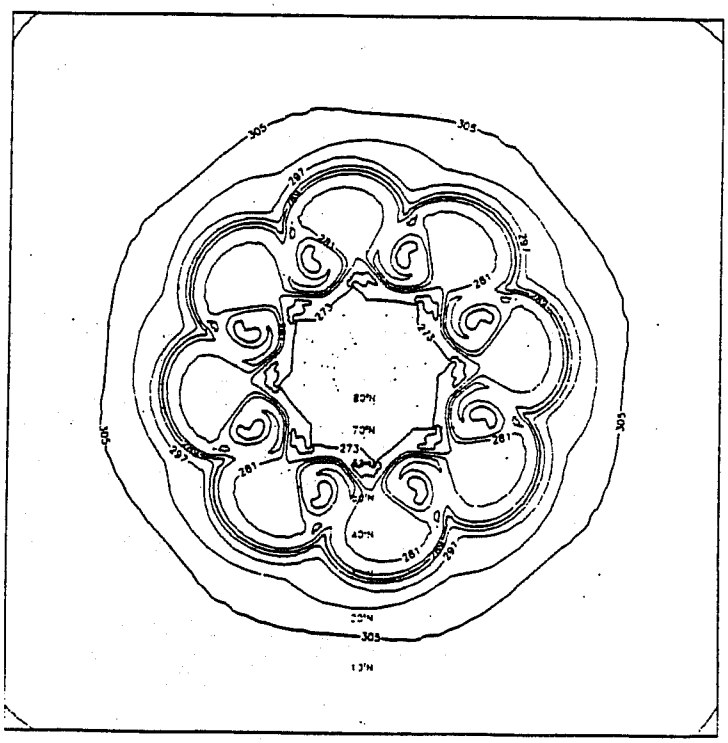

Fig. 5 : *As Figure 4 but T106L19C1.*

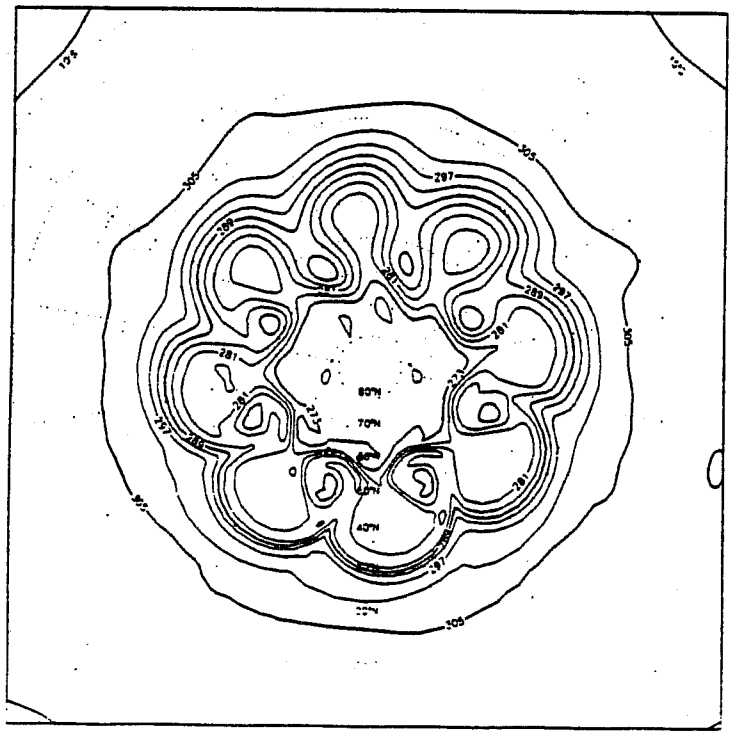

Fig. 6 : *As Figure 4 but T42L19C3.*

forecast is likely to be also valuable in the medium range, especially with a low stretching factor and keeping the pole of stretching at the northern pole. We intend to study in the coming year the impact of the variable resolution on the model's climate, which could be useful for climatic applications but which is also essential to understand the long term behaviour of the data assimilation.

3 Data assimilation.

In the Arpege/IFS system, emphasis has been put, at the research level, on data-assimilation. An optimal interpolation and a 3D-Var assimilation schemes are implemented which are both are under scientific evaluation. Concerning the time dimension, both a Kalman filter and a 4D-Var scheme are implemented (3D-VAR is indeed coded as the particular case of 0 time step of the model). We present in the following results on 4D-VAR.

3.1 Feasibility study of 4-D Var.

A feasibility study of 4D-Var has been conducted in summer and fall 1990. The results are positive, we refer to Thépaut and Courtier (1991) for a presentation of these results.

3.2 4-D Var in presence of baroclinic instability.

The baroclinic instability case studied.

As in Thépaut and Courtier (1991), the primitive equation model used in this study is a T21L19 version, the number of degrees of freedom of the model is thus 28072. The same basic zonal state as in section 2.8.2 is used. The nonlinear evolution of the baroclinic wave is simulated by integrating the model for fifteen days from initial conditions consisting of the zonal flow perturbed by the most unstable mode at zonal wavenumber 6. This mode is scaled as to give 1 hPa maximum amplitude for the surface pressure.

The results are consistent with SH78: after nine days of growth where the minimum value of the surface pressure drops from 1008 hPa to 972 hPa, barotropic effects induce a decay of the wave and a corresponding increase of the value of the maximum wind. The most intense cyclogenesis occurs between days 6 and 8 with a maximun drop in surface pressure of 8 hPa per day. On the seventh day of the life cycle, the wave exhibits a structure characteristic of occluding systems at midlatitudes (Figure 7 to be compared with Figure 1 of SH78).

The experiments.

The assimilation problem is to find the initial conditions of a numerical forecast, taking into account

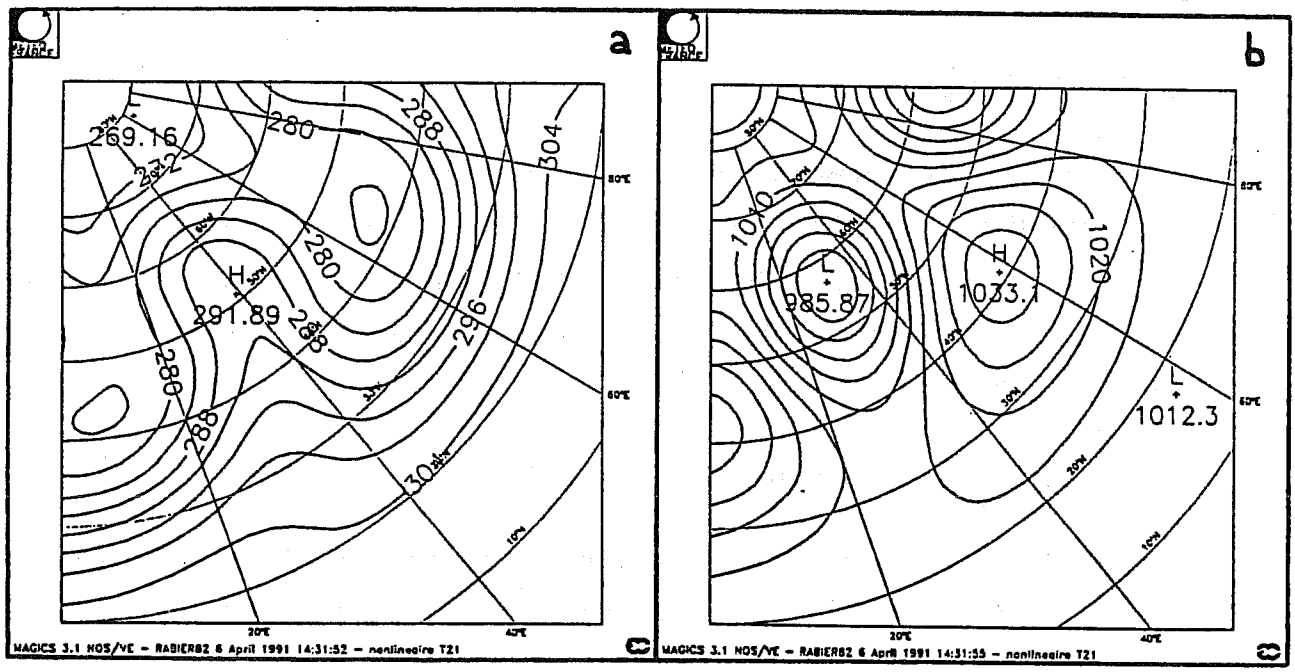

Fig. 7 *Temperature at the lowest level (panel(a)) and surface pressure (panel(b)), at day 7. Contour intervals are 4 K for the temperature and 5 hPa for the surface pressure.*

all prior information on the atmospheric state. 4D-VAR approach consists in using the dynamical information through the model equations by finding the model trajectory that lies as close as possible to the available data over a time period (t_0, t_n).

In the following, the assimilation period generally spans 24 hours from day 6 to day 7, during which the cyclogenesis is the most intense. The observations are model states in spectral space, extracted from the reference trajectory given by the fifteen day run. In this adiabatic problem, they simply consist of the spectral components of vorticity, divergence, temperature and of the logarithm of the surface pressure. We assume that observations are available at every time step, i.e. at a frequency of forty minutes at truncation T21.

The cost function to be minimized is

$$J(x(t_0)) = \frac{1}{2}\sum_{i=0}^{n} < x(t_{i/n}) - x_{ref}(t_{i/n}), x(t_{i/n}) - x_{ref}(t_{i/n}) > \qquad (72)$$

where $x(t_{i/n})$ stands for the model state at time $t_{i/n}$ and $x_{ref}(t_{i/n})$ for the reference state at the same time. The inner product is the one associated with the norm energy. In the experiments, according to which part of the flow is supposed to be observed, only certain spectral components will be taken into account in this cost function. The inner product energy is also used for defining the metric in the minimization space. The minimization algorithm is of a mixed quasi-Newton/conjugate gradient type described in Buckley and Lenir (1983) and implemented by "Institut National de la Recherche en Informatique et Automatique".

Observation of the evolution of the eddy part of the flow.

The idea of this first series of experiments is to test the assimilation method in a "theoretical" situation where the eddy part of the flow is assumed to be observed whereas the zonal part of the flow is not. It should be noted that this simulation is not totally meaningless from a meteorological point of view. As a matter of fact, ground networks depict reasonably well the surface eddies but the lack of upper-air observations fails to give a satisfactory description of great structures such as the mid-latitude upper jets.

For the different variables, the observations consist of all the zonal wavenumbers m except $m = 0$: all but the zonal components of the flow. Is it then possible to retrieve the zonal part of the flow from the observation of the temporal evolution of the eddy part of the flow?

In a first experiment the initial point of the minimization is the atmospheric state at day 4 (Figure 9), whose zonal part is significantly different from the desired result (Figure 8) although its structure is comparable. The main differences between the two fields are located at the lowest levels. At day 6, winds have become stronger below the jet and easterlies have spread on both sides of it. Between day 4 and day 6 the maximum difference in zonal winds is of 2.90 ms^{-1}, and in temperature

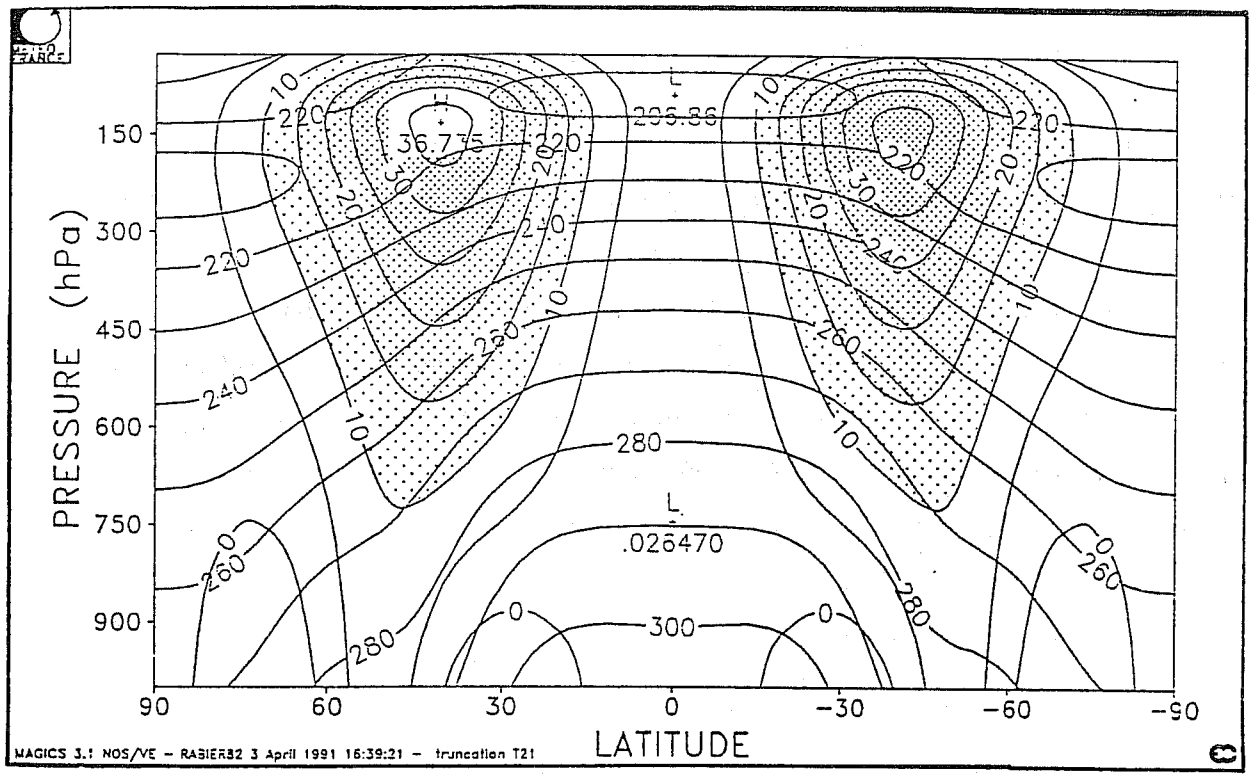

Fig. 8 *Latitude-height section (as in Fig.3) showing the reference situation: day 6 of the life cycle.*

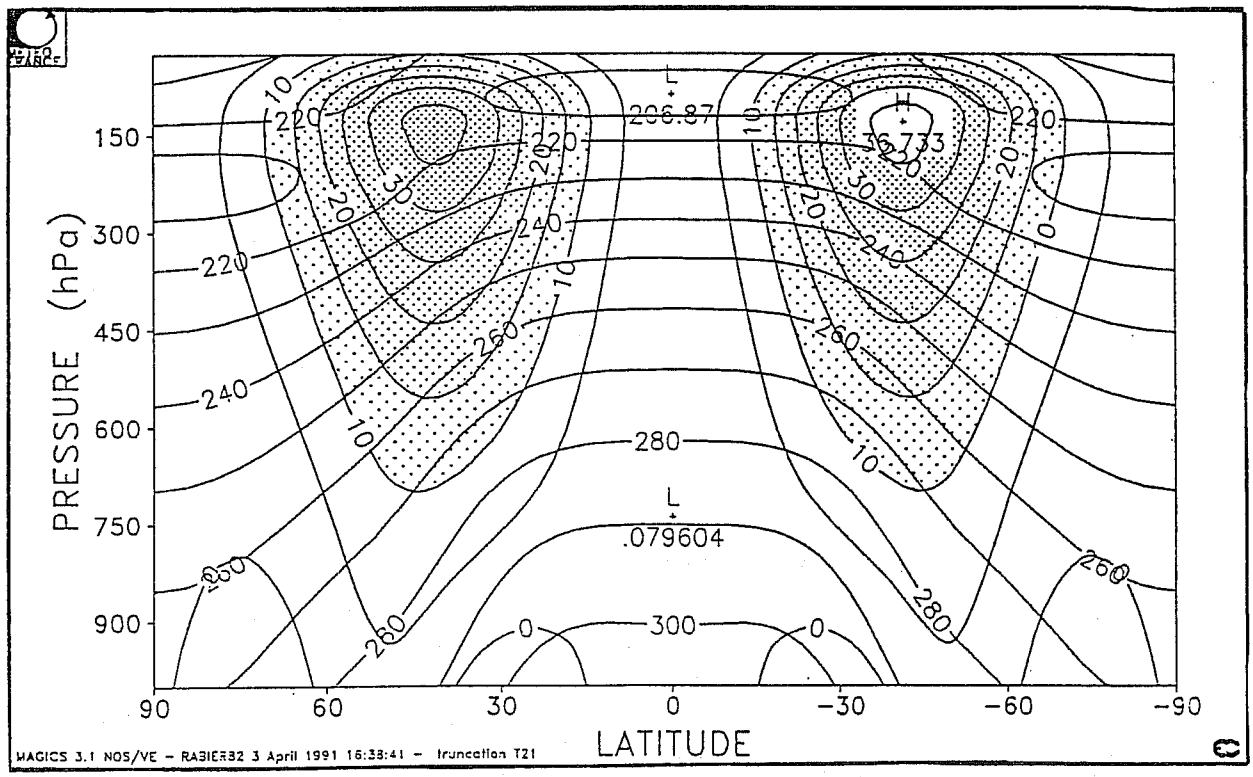

Fig. 9 *Latitude-height section (as in Fig.3) showing the starting point of the minimization: day 4 of the life cycle.*

2.37 K. The algorithm performs well; the cost function is divided by 5 orders of magnitude after 30 iterations and the global distance between the zonal part of the result and the truth is divided by a factor of 2.4. Figure 10 compares well with reality (Figure 8). Winds over 5 ms^{-1} now reach the ground at midlatitudes. In terms of difference to truth, the wind RMS has decreased from 0.36 ms^{-1} to 0.23 ms^{-1} at high altitude (250 hPa), and from 1.11 ms^{-1} to 0.38 ms^{-1} at 1000 hPa. Accordingly, the temperature RMS has dropped from 0.12 K to 0.07 K at 250 hPa and from 0.94 K to 0.35 K at 1000 hPa.

The following step is to start the minimization from an atmospheric state much different from the reference one, taking a state of rest with the standard atmospheric structure of temperature and a uniform standard pressure. The maximum difference in zonal winds now reaches 36 ms^{-1}, and 18 K in temperature. When performing the assimilation the convergence is very slow. No less than 150 simulations are necessary to reach a relative saturation of the minimization. The problem beneath this slowness is the fact that two distinct parts of the control variable are treated jointly: the eddy part of the flow which is fully observed and the zonal part of the flow for which the information is indirect, through dynamical links. In the preceding experiment, those two components were present but the starting point of the minimization was close enough to ensure a quick convergence. Presently, at such a distance from the truth (more than twenty times further than in the previous experiment), treating two components of the control variable that have such different impacts on the cost function leads to a classical narrow valley conditioning problem. To speed up convergence we chose to perform the minimization only with respect to the zonal part of the flow, the eddy part being set equal to truth at the beginning of the minimization. Compared with the ill-conditioned case, the behaviour is greatly improved as the distance to truth reached after 30 simulations is slightly smaller to what was achieved after 150 simulations previously. From Figure 11 one sees that the result of the minimization is encouraging. The important features of the flow at mid-latitudes, i.e. the tropospheric jet in conjunction with the thermal meridional gradient, are reproduced. The global RMS of zonal wind error has decreased from 8.61 ms^{-1} to 2.72 ms^{-1} and the global RMS of mean zonal temperature has dropped from 9.25 K to 5.66 K. However, differences can be seen in the tropics at low levels and at high latitudes.

Does the assimilation period length affect the results? This is investigated varying it from 12 to 72 hours. The square of the distances between reality and the result of the minimization after 30 simulations are 7.89 10^6, 7.46 10^6, 7.47 10^6 and 9.94 10^6 for 12, 24, 48 and 72 hours. Plotting the values of the cost functions according to the number of simulations also gives an idea of the rate of decrease (Figure 12). For ranges up to 48 hours, the longer the assimilation period is, the better the

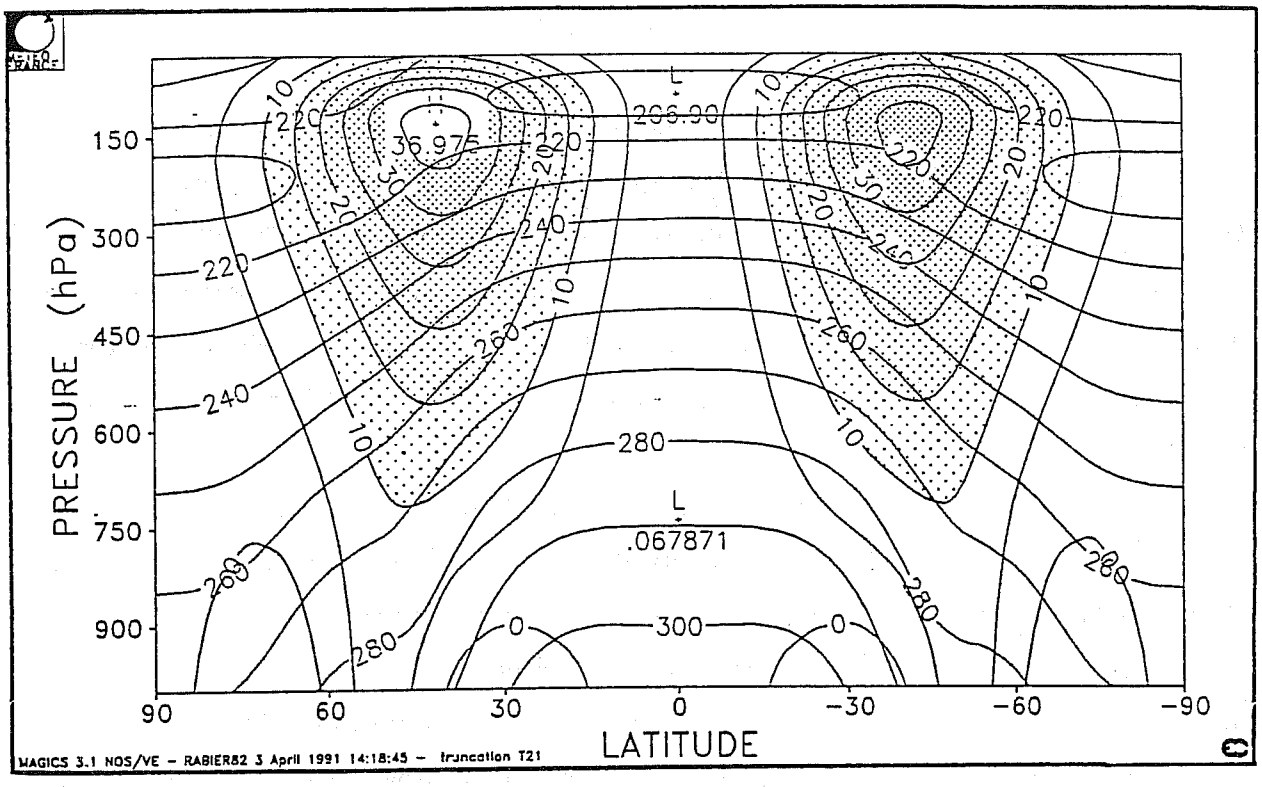

Fig. 10 *Latitude-height section (as in Fig.3) showing the result of the assimilation after 30 simulations. The starting point of the minimization is day 4. Observations consist of all zonal wavenumbers except m = 0 for all the model variables, at each time step for an assimilation period of 24 hours (day 6 to day 7).*

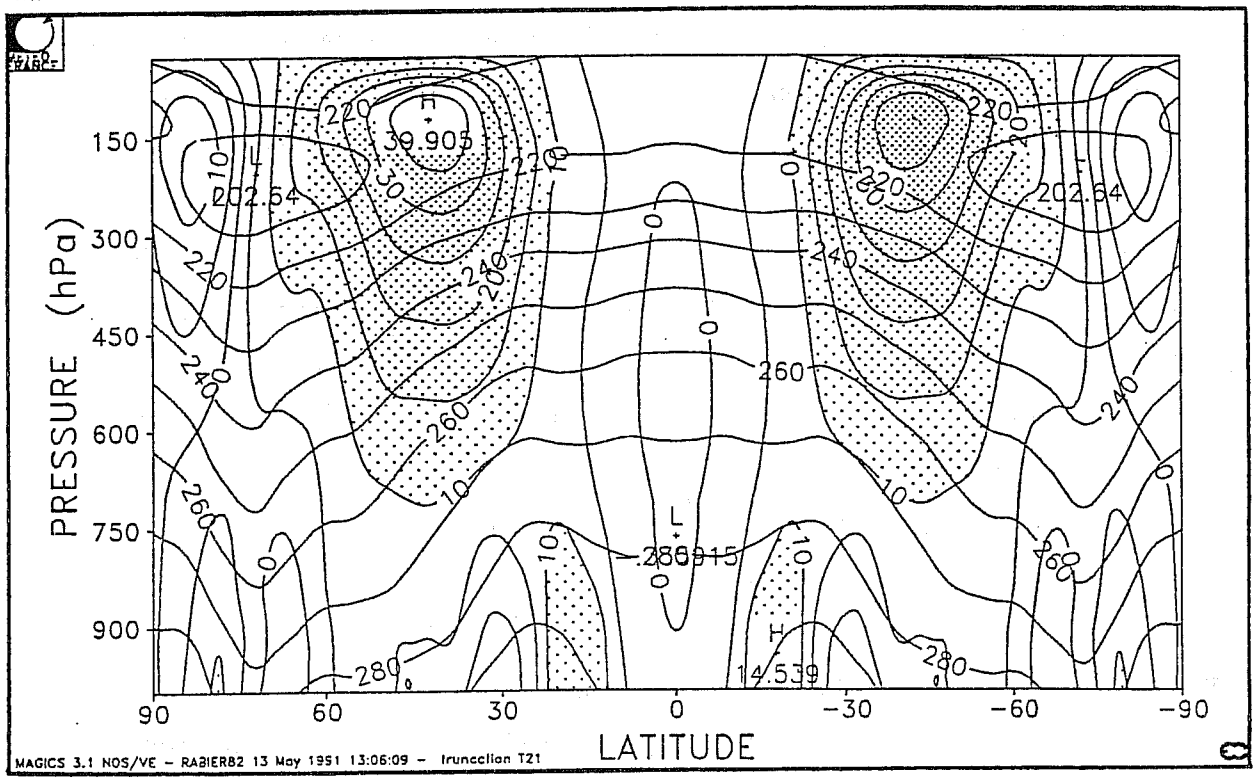

Fig. 11 *Latitude-height section (as in Fig.3) showing the result of the assimilation after 30 simulations. Starting point of the minimization: state of rest, standard temperature and standard pressure for the zonal part of the flow; the same as the reference situation for the eddy part of the flow. Observations: all zonal wavenumbers except m = 0 for all the model variables, at each time step for an assimilation period of 24 hours (day 6 to day 7). The minimization is performed only with respect to the zonal part of the flow.*

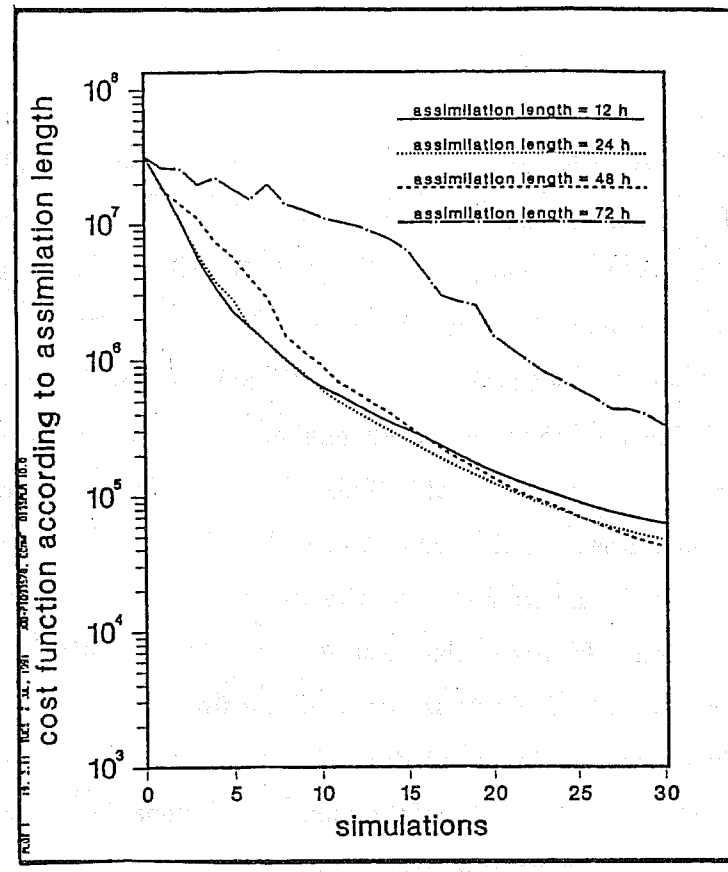

Fig. 12 *Values of the cost function for different assimilation period lengths according to the number of simulations. Starting point of the minimization: state of rest, standard temperature and standard pressure for the zonal part of the flow; the same as the reference situation for the eddy part of the flow. Observations: all zonal wavenumbers except m = 0 for all the model variables, at each time step for an assimilation period of 24 hours (day 6 to day 7). The minimization is performed only with respect to the zonal part of the flow.*

Curve (o): assimilation period length = 12 hours. Curve (+): assimilation period length = 24 hours. Curve (∗): assimilation period length = 48 hours. Curve (×): assimilation period length = 72 hours.

The curves are scaled as to start from the same value at the initial time of the assimilation.

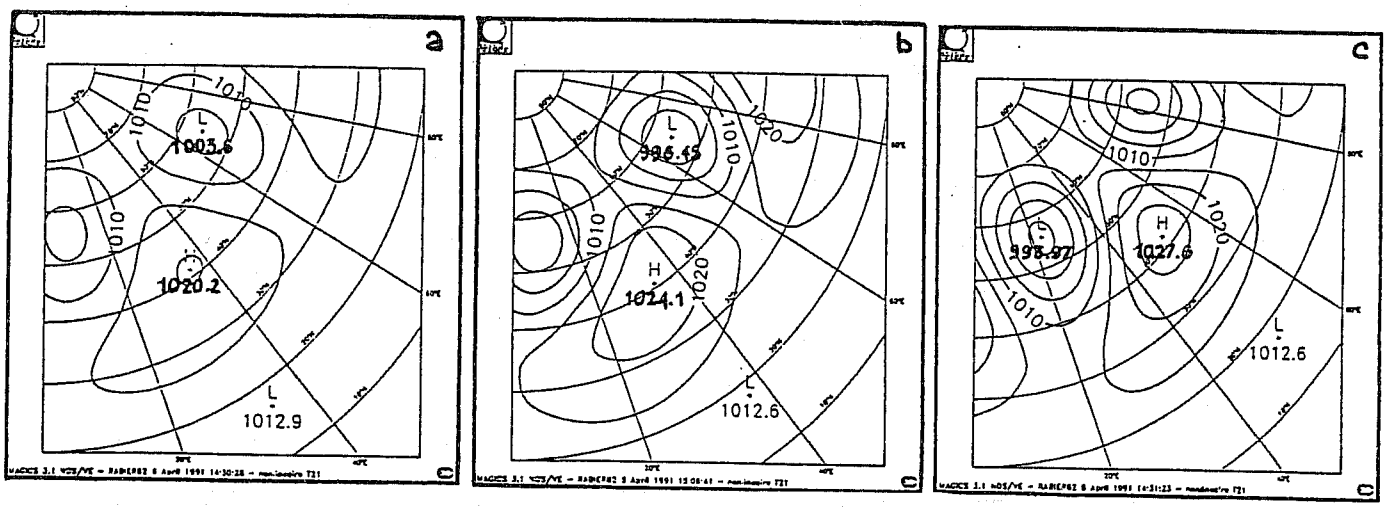

Fig. 13 *Results of the assimilation for the surface pressure after 30 simulations when observations consist of all zonal wavenumbers except m = 6 for all the model variables, at each time step for an assimilation period of 24 hours (day 6 to day 7). Panel (a) shows the starting point of the minimization: day 4 of the life cycle.*

Panel (b) shows the result of the minimization.

Panel (c) shows the reference field.

result because more information is present. One could notice that at the end of the minimization, the distance with reality is slightly higher for the 48 hour period than for the 24 hour period, but the rate of decrease of the cost function is significantly higher which ensures the superiority of this assimilation period after a few more iterations. For longer periods than 72 hours, it can be shown that nonlinearities become a dominant part of the dynamics. These nonlinearities induce a non-quadraticity of the cost function and thus a much more difficult minimization. This can be seen on the behaviour of the descent algorithm which is rather chaotic. Two trials are sometimes necessary for a line search along the descent direction. However, after 20 to 30 simulations, the rate of decrease is considerably higher for the 72 hour assimilation period than for the others. In constrast with what happens for the 12 hour period, minimization is far from being saturated after 30 simulations.

Observation of the evolution of the zonal part of the flow.

Another question of interest in the assimilation of meteorological observations is addressed: can perturbations be derived from the knowledge of the atmospheric global features? Symmetrical to what was accomplished in the preceding series of experiments, the observations now include all the zonal wavenumbers of the variables except $m = 6$, which characterizes the synoptic perturbations present in the atmospheric flow. Is it possible to retrieve the eddies from the observation of the temporal evolution of the zonal part of the flow and from the observation that no energy is present in zonal wavenumbers different from $m = 0$ or $m = 6$?

The first experiment, started from the atmospheric state at day 4 exhibits results that may look surprising. There is a decrease in the cost function and a paradoxal increase in the distance between the result of the minimization and reality. The interpretation can be found in Figure 13. The eddy intensity of the result of the assimilation process is approximately correct, but the pattern is totally out of phase. The dynamics included in the assimilation method are able to infer the development of the perturbation from the temporal evolution of the zonal part of the flow. The minimum surface pressure has dropped by 7 hPa from 1003.6 hPa in the starting point of the analysis to 996.4 hPa. However, due to the symmetry of the problem, it is clear that the feedback of the perturbation on the zonal part of the flow is independent of its location in longitude. The location of the perturbation given by the initial point of the minimization (day 4) is kept unchanged.

Now, if no information at all is given on the location of the perturbation, neither in the assimilation process nor in the initial point of the minimization (the zonal part of the flow at day 6), the algorithm fails to find a minimum. This is typically a case where the cost function possesses multiple minima, as can be seen in Figure 14 which is a cross section of the cost function along the direction of the perturbation. For the perturbation itself, the value is stricly zero, but for minus the perturbation

which roughly corresponds to a $\frac{\pi}{6}$ shift in longitude, the cost function is also very close to zero.

The next experiment is designed to solve this problem of undetermined location of the perturbation, with as little additional information as possible. For the three dimensional fields (vorticity, divergence and temperature) the observations are, as before, all the zonal wavenumbers except $m = 6$. But for the surface pressure, which can be considered to be well observed in the meteorological reality, the first total wavenumbers from $n = 0$ to $n = 8$ and all the zonal wavenumbers associated with them are supposed to be known. It is of importance to note that observing up to $n = 8$ for the surface pressure gives information on only 36% of the energy of the perturbation of this field in this particular experiment. The starting point of the minimization is the zonal part of the flow at day 4 of the life cycle.

As can be seen in Figure 15, the results are very good. Starting from an unperturbed zonal field and observing only a part of the perturbation (panel (a)), the pattern obtained after 30 simulations (panel (b)) is in good agreement with reality (panel(c)). The streamfunction at the last level of the model (closest to the ground) for which no component is observed (not shown) is also well reconstructed. Although these results are really satisfactory, it should be noted that convergence is not yet achieved and that after 60 simulations the analysis is even better (not shown). For example the shapes of the 1015 hPa and 1010 hPa contours get closer to the reference situation.

Discussion

This series of results clearly shows the potential of 4D-VAR. The purely nonlinear feedback that exists between the perturbation and the zonal part of the flow is correctly treated. Once a piece of information on the location of the perturbation is present in the observations or in the starting point of the minimization, the eddy part of the flow is correctly derived from the temporal evolution of the zonal part of the flow and vice-versa, the observation of the evolution of the eddy component of the flow is enough to infer the zonal structure and in particular the presence of the jet.

3.3 Kalman filter.

Kalman filter is currently being used to demonstrate with the vorticity equation the potential of a space based doppler wind lidar. In addition we perform a comparison of 4D-VAR versus Kalman filter and we evaluate the impact of the proper treatment of the time dimension.

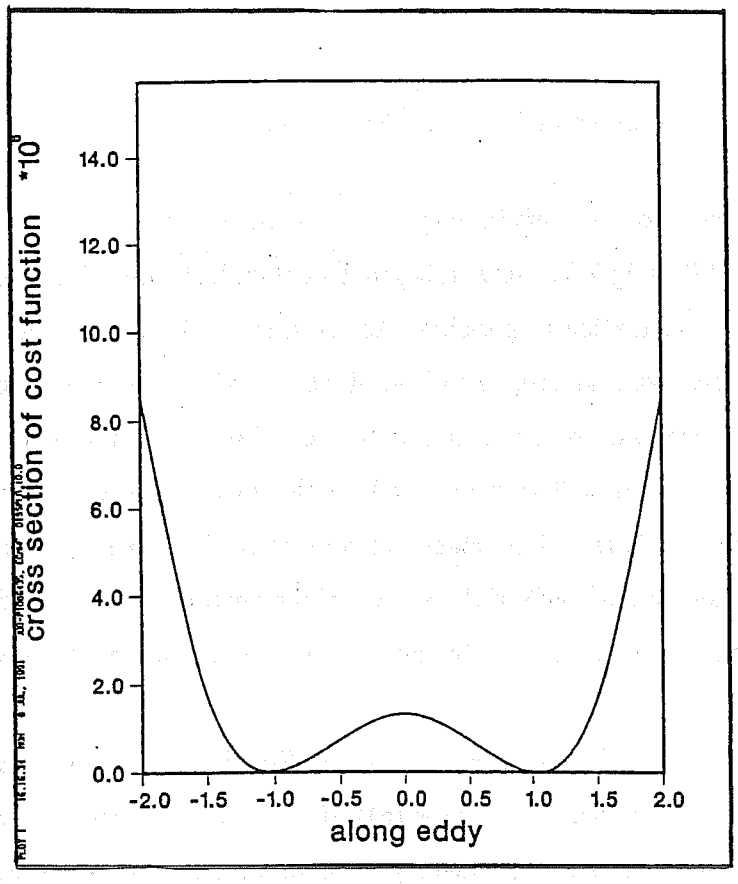

Fig. 14 *Cross section of the cost function along the direction of the perturbation: values of the cost function measuring the discrepancy between the reference run and the model run taking into account all components of the flow except $m = 6$, when the model is started from the zonal part of the flow at day 6 to which α times the eddy part of the flow at day 6 is added.*

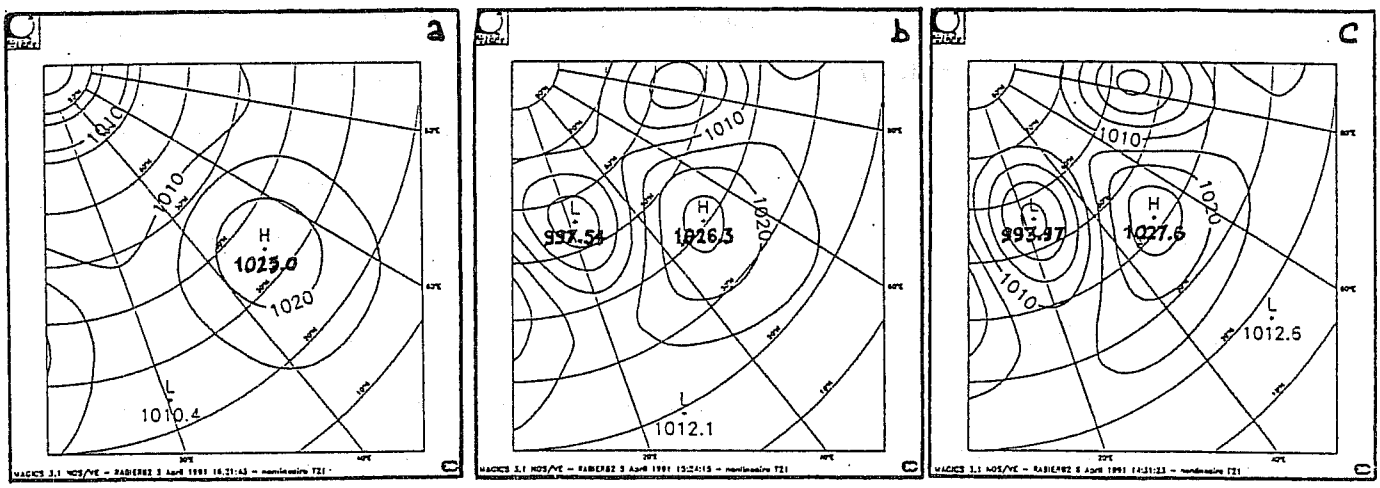

Fig. 15 *Results of the assimilation for the surface pressure after 30 simulations, starting from the zonal part of the flow at day 4. Observations consist of all zonal wavenumbers except $m = 6$ for all the model variables, except for the surface pressure for which all total wavenumbers from $n = 0$ to $n = 8$ (with the corresponding zonal wavenumbers) are observed. The frequency and period of observation is the same as before.*

Panel (a) shows the observations for the surface pressure at the first time step.

Panel (b) shows the result of the minimization.

Panel (c) shows the reference field.

4 Conclusion.

Most of the code is already developed and the Arpege team is now undergoing scientific validation. The operational implementation should be achieved in two steps. Firstly, EMERAUDE will be replaced by the Arpege code but in an equivalent configuration (T79L15C1) during spring 1992. Secondly, the major scientific step (replacing PERIDOT by Arpege) should take place during the last quarter of 1992, the replacement of the optimal interpolation scheme by 3D-Var being for Spring 1993.

On the scientific side as main points, the validation of Arpege in climatic mode will be done in early 1992 by a 10 year run in T42L30C1 with an interactive ozone. The use of real observation in 4D-Var is already possible and scientific results should come soon.

5 References.

Asselin, R. A., 1972: Frequency filter for time integration. *Mon. Wea. Rev.*, **100**, 487–490.

Bezold, W. von, 1888: Zur Thermodynamik der Atmosphäre. *Sitzber. Ak. Berlin*, **21**, 485–522.

Boer G. J., N. A. McFarlane, R. Laprise, J. D. Henderson and J. P. Blanchet, 1984: The Canadian Climate Centre spectral atmospheric general circulation model. *Atmos. Ocean*, **22**, 397–429.

Bougeault, P., 1985: Parameterization of cumulus convection for GATE. A diagnostic and semi-prognostic study. *Mon. Wea. Rev.*, **113**, 2108–2121.

Buckley, A., and A. Lenir, 1983: QN-like variable storage conjugate gradients. *Mathematical Programming*, **27**, 155–175.

Cariolle D., A. Lasserre-Bigorry, J. F. Royer and J. F. Geleyn, 1990: A general circulation model simulation of the springtime Antartic ozone decrease and its impact in midlatitudes. *J. Geophys. Res.*, **95**, 1883–1898.

Coiffier J., Y. Ernie, J. F. Geleyn, J. Clochard, J. Hoffman and F. Dupont, 1987: The operational hemispheric model at the French meteorological service. *J. Meteor. Soc. Japan*, **Special NWP symposium issue**, 337–345.

Courtier, P. and J. F. Geleyn, 1988: A global numerical weather prediction model with variable resolution: Application to the shallow-water equations. *Quart. J. Roy. Meteor. Soc.*, **114**, 1321–1346.

Deardorff, J. W., 1978: Efficient prediction of ground surface temperature and moisture, with inclusion of a layer of vegetation. *J. Geophys. Res.*, **83**, 1889–1903.

Ducrocq, V., and P. Bougeault, 1990: *La ligne de grain du 7 juin 1987, résultats du modèle PERIDOT - "10 km"*. Notes de recherche n^o1, Météo-France, Paris, 126 pp.

Eliasen, E., B. Machenhauer and E. Rasmussen, 1970: *On a numerical method for integration of the hydrodynamical equations with a spectral representation of the horizontal fields.* Report n°2, København universitet, Institut for Teoretisk Meteorologi, 35 pp.

Freydier C., 1991: *Instabilité barocline et maille variable.* Rapport de DEA, Université Pierre et Marie Curie, Paris, 38 pp.

Geleyn, J. F., 1987: Use of a modified Richardson number for parameterizing the effect of shallow convection. *J. Meteor. Soc. Japan*, **Special NWP symposium issue**, 141–149.

Geleyn, J. F., 1988: Interpolation of wind, temperature and humidity values from model levels to the height of measurement. *Tellus*, **40A**, 347–352.

Geleyn, J. F., and A. Hollingsworth, 1979: An economical analytical method for the computation of the interaction between scattering and line absorption of radiation. *Beitr. Phyz. Atmosph.*, **52**, 1–16.

Geleyn, J. F., C. Girard and J. F. Louis, 1982: A simple parameterization of moist convection for large-scale atmospheric models. *Beitr. Phyz. Atmosph.*, **55**, 325–382.

Geleyn, J. F., M. J. Rochas and P. Courtier, 1991: Special features of the unparameterized set of equations for the "Arpege" NWP system at DMN. To appear in *Proceedings of the ninth A.M.S. Conference on N.W.P., Denver.*

Gill, A. E., 1982: *Atmosphere-Ocean dynamics.* Academic Press, 662 pp.

Hortal, M., 1991: Formulation of the ECMWF model (same volume).

Hortal, M., and A. J. Simmons, 1991: Use of reduced gaussian grids in spectral models. Mon. Wea. Rev., **119**, 1057–1074.

Imbard, M., A. Craplet, P. Degardin, Y. Durand, A. Joly, N. Marie and J. F. Geleyn, 1987: Fine mesh limited area forecasting with the French operational Peridot system. *Proceedings of the 1987 ECMWF seminar on the nature and prediction of extra-tropical weather systems.*, **II**, 231–270.

Kalnay, E., and M. Kanamitsu, 1988: Time schemes for strongly nonlinear damping equations. *Mon. Wea. Rev.*, **116**, 1945–1958.

Kalnay, E., M. Kanamitsu, J. Pfaendtner, J. Sela, M. Suarez, J. Stackpole, J. Tucillo, L. Umscheid and D. Williamson, 1989: Rules for interchange of physical parameterizations. *Bull. Am. Meteor. Soc.*, **70**, 620–622.

Louis, J. F., M. Tiedke and J. F. Geleyn, 1982: A short history of the PBL parameterization at ECMWF. *Proceedings of the ECMWF workshop on planetary boundary layer parameterization*, Reading, 25-27 Nov. 1981, 59–80.

Marquet, P., 1991: *Initialisation dans Arpege.* To appear in Note de travail Arpège, Météo-France, Paris.

Orszag, S. A., 1970: Transform method for calculation of vector coupled sums: application to the spectral form of the vorticity equation. *J. Atmos. Sci.*, **27**, 890–895.

Ritter, B., and J. F. Geleyn, 1991: A comprehensive radiation scheme for numerical weather prediction models with potential applications in climate simulations. To appear in *Mon. Wea. Rev.*

Robert, A. J., 1982: A semi-Lagrangian and semi-implicit numerical integration scheme for the primitive meteorological equations. *J. Meteor. Soc. Japan*, **60**, 319–324.

Rochas, M., K. Yessad and J. Clochard, 1991a: *Transformations de sphère à sphère. Rotations et dilatations dans l'espace spectral.* Note de travail "Arpege" n° 19, Météo-France, Paris, 51 pp.

Rochas, M., P. Courtier, K. Yessad and Y. Bouteloup, 1991b: Rotations in spectral space. To appear in *Beitr. Phyz. Atmosph.*

Rochas, M., M. Imbard, A. Craplet and P. Duhaut, 1991c: Semi-implicit and Semi-Lagrangian advection schemes for spectral models of the shallow-water equations. Submitted to *Mon. Wea. Rev.*

Schmidt, F., 1977: Variable fine mesh in spectral global model. *Beitr. Phyz. Atmosph.*, **50**, 211–217.

Simmons, A. J., and B. J. Hoskins, 1978: The life cycles of some nonlinear baroclinic waves *Quart. J. Roy. Meteor. Soc.*, **35**, 414–431.

Simmons, A., and D. Burridge, 1981: An energy and angular momentum conserving vertical finite difference scheme and hybrid vertical coordinates. *Mon. Wea. Rev.*, **109**, 758–766

Temperton, C., 1989: Implicit normal mode initialization for spectral models. *Mon. Wea. Rev.*, **117**, 436–451.

Temperton, C., 1991: On scalar and vector transform methods for global spectral models. *Mon. Wea. Rev.*, **119**, 1303–1307.

Thépaut, J. N., and P. Courtier, 1991: Four dimensional variational data assimilation using the adjoint of a multilevel primitive equation model. To appear in *Quart. J. Roy. Meteor. Soc.*

6 Aknowledgments.

The authors would like to thank the Arpege and IFS teams. Among others, we are embeded to Maurice Imbard for the semi-Lagrangian experiments, to Yves Bouteloup for variable resolution experiments, to Jean-Noël Thépaut for 4D-VAR results, to Pierre Gauthier for Kalman filter runs and to Pascal Marquet for Nonlinear Normal Mode Initialisation experiments.

In addition we recall again that the code has been developed through a collaboration with ECMWF and Mats Hamrud must be aknowledged for his major contribution.